

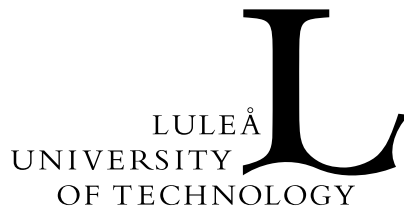
# Dust in the Early Universe

Erik Elfgren

Luleå University of Technology  
Department of Applied Physics and Mechanical Engineering  
Division of Physics

2005:17 | ISSN: 1402-1757 | ISBN: LTU-LIC -- 05/17 -- SE





# Dust in the Early Universe

Erik Elfgren

Division of Physics  
Department of Applied Physics and Experimental Mechanics  
Luleå University of Technology  
SE-971 87 Luleå  
Sweden

Luleå 2005

**Dust**

And dance as dust before the Sun,  
And light of foot and unconfined,  
Hurry from road to road, and run  
About the errands of the wind.

And every mote, on earth or air,  
Will speed and gleam, down later days,  
And like a secret pilgrim fare  
By eager and invisible ways,

Nor ever rest, nor ever lie,  
Till, beyond thinking, out of view,  
One mote of all the dust that's I  
Shall meet one atom that was you.

- *Rupert Brooke (1887-1915)*

# Preface

The work presented in this Licentiate thesis is a result of a collaboration between Luleå University of Technology, Laboratoire d'Astrophysique de l'Observatoire de Grenoble, Institut d'Astrophysique de Paris and Centre de Recherche Astronomique de Lyon. My supervisor at Luleå University of Technology has been Sverker Fredriksson and my co-supervisor has been Johnny Ejemalm.

I would like to express my gratitude towards the world in general for being such a beautiful place, and towards my collaborators in particular for having helped me in my quest for knowledge and understanding of the workings of the universe. Of my collaborators I especially would like to thank François-Xavier Désert for his ideas, his concrete approach to problem solving and all the verifications he proposed to corroborate our results. Furthermore, I thank Bruno Guiderdoni for his invaluable support in the field of dark matter simulations. Of course, my supervisor Sverker Fredriksson has been of much help with his good general knowledge of astrophysics.

I am grateful to my office-mate, Fredrik Sandin, for our discussions and his help with practical as well as theoretical issues and to Tiia Grenman and Johan Hansson for the exchanges we have had. I would also like to thank Henrik Andréén for his help in the matter of geometry and to all my friends for our friendship.

Finally, a special thank goes to my wonderful, supporting wife, who is with me in my moments of defeat as well as of victory and to my parents, who have brought me up to who I am today.

Luleå in March 2005

Erik Elfgren



# Abstract

This Licentiate thesis treats the impact of early dust on the Cosmic Microwave Background (CMB). The dust that is studied comes from the first generation of stars, which were hot and short-lived, ending their lives as giant supernovæ. In the supernova explosions, heavy elements, produced through the fusion in the stars, were ejected into the interstellar medium. These heavy elements condensed to form dust, which can absorb and thus perturb the Cosmic Microwave Background radiation. The dust contribution to this radiation is calculated and found negligible. However, as the dust will be produced within structures (like galaxy clusters), it will have a spatial correlation that could be used to detect it. This correlation is calculated using relevant assumptions. The planned Planck satellite is likely to be able to measure and thus confirm this correlation.

Keywords: *Dust – CMB – Reionization – Power spectrum*





# Papers

The following papers are appended to this Licentiate thesis:

*Paper I: **Dust from Reionization***

The production of dust in the early universe is estimated from the number of stars needed to achieve reionization. The spectral signature of the dust is calculated and compared to measurements. The contribution from the dust layer to the Cosmic Microwave Background is found to be small.

Published: Elfgrén, Erik and Désert, François-Xavier, 2004, *Astronomy and Astrophysics*, **425**, 9-14.

*Paper II: **Dust Distribution During Reionization***

The spatial distribution of the dust is estimated using simulations of dark matter density evolution. Combining the calculated intensity from Paper I with this density and integrating along the line of sight, the spatial signature of the dust is obtained. The distribution of the dust gives a detectable signal.

Submitted to *Astronomy and Astrophysics*.



# Contents

<b>1</b>	<b>Introduction</b>	<b>1</b>
<b>2</b>	<b>History of the Universe</b>	<b>3</b>
2.1	The Big Bang . . . . .	3
2.2	Inflation . . . . .	3
2.3	Radiation Dominated Era . . . . .	5
2.4	Matter Dominated Era . . . . .	5
2.5	Decoupling of Matter . . . . .	6
2.6	Structure Formation . . . . .	6
2.7	The First Generation of Stars . . . . .	6
2.8	Reionization . . . . .	7
<b>3</b>	<b>The Cosmic Microwave Background</b>	<b>9</b>
3.1	Primary Anisotropies . . . . .	10
3.1.1	Gravitational Anisotropies . . . . .	11
3.1.2	Adiabatic Anisotropies . . . . .	11
3.1.3	Doppler Anisotropies . . . . .	11
3.2	Secondary Anisotropies . . . . .	11
3.2.1	Gravitational Effects . . . . .	11
3.2.2	Local Reionization . . . . .	12
3.2.3	Global Reionization . . . . .	12
3.3	Foregrounds . . . . .	13
3.3.1	Extragalactic Foregrounds . . . . .	13
3.3.2	Galactic Foregrounds . . . . .	13
3.3.3	Local Foregrounds . . . . .	14
3.4	Power spectrum . . . . .	14
3.4.1	Acoustic Oscillations . . . . .	14
3.4.2	Simulations of the CMB . . . . .	15
<b>4</b>	<b>Short Introduction to the Papers</b>	<b>17</b>
4.1	Dust . . . . .	17
4.1.1	Production . . . . .	17
4.1.2	Properties . . . . .	17
4.1.3	Destruction . . . . .	18
4.2	Dark Matter . . . . .	18

<b>5</b>	<b>Summary and Outlook</b>	<b>21</b>
5.1	Summary . . . . .	21
5.2	Outlook . . . . .	22
<b>A</b>	<b>Cosmology</b>	<b>25</b>
A.1	Basic Introduction . . . . .	25
A.2	Cosmological Equations . . . . .	26
<b>B</b>	<b>Explanations</b>	<b>27</b>
B.1	Glossary . . . . .	27
B.2	Abbreviations . . . . .	29
B.3	List of Variables . . . . .	29
B.4	List of Cosmological Constants . . . . .	30
B.5	List of Physical Constants and Units . . . . .	30
<b>C</b>	<b>Appended Papers</b>	<b>31</b>

# Chapter 1

## Introduction

The Universe is a wonderful place. Ranging from smaller than an atom to larger than a galaxy, with complex humans, beautiful flowers, powerful stars, and vast amounts of empty space. But where does it all come from? How did all this diversity come to be?

The universe is generally believed to have started out in the Big Bang – an immense concentration of energy, expanding and thus diluting. Different particles were created such as neutrons, protons and electrons, then ions and atoms. A long pause followed during which matter assembled through gravity to form large-scale structures such as stars and galaxies. And in the galaxies, around the stars, planetary systems assembled which can host life.

But how can we know all this? The truth is that we do not. However, we do have several pieces of indirect evidence. The single most important observation is the so called Cosmic Microwave Background radiation (CMB for short). This radiation was emitted when the universe was merely 300,000 years old and can be thought of as a kind of photograph taken of the universe at this time. Amazing! Furthermore, this radiation is present everywhere in the universe and has a very characteristic spectrum. The discovery of the CMB single-handedly convinced the scientific community of the validity of the Big Bang model.

In order to measure the CMB accurately, we must know what it has passed through; our solar system, our galaxy, other galaxies, further and further away until the first generation of stars. Very little is known about these first stars. One plausible hypothesis states that they had very intense and violent lives. This would mean that they finished as supernovae – giant explosions – thus spreading their contents in space. These left-overs are called star dust, and due to its abundant production and wide spread it will partly cloud the CMB. It is like looking at the Sun through a mist.

In this Licentiate thesis I try to assert the thickness, density and distribution of this dust layer, thus evaluating its impact on the measurements of the CMB. As a corollary, certain properties of the first generation of stars could also be obtained.

In the second chapter, the early history of the universe is outlined, from the Big Bang until the formation of the first galaxies. In the third chapter the Cosmic Microwave Background with its properties and its different foregrounds is described in some detail. In the fourth chapter, I present a brief introduction that is useful for the understanding of some of the particulars of the two appended papers. This includes a description of our general knowledge of dust and some concepts of dark matter.

In appendix A a short introduction to cosmology is provided along with some common formulæ. For further details on symbols, constants, and abbreviations, see Appendix B. Words which appear *slanted* are explained in the Glossary in the same appendix.



## Chapter 2

# History of the Universe

Our understanding of the evolution of the universe is far from complete, but the picture is getting clearer by the day with the advent of new detectors and new experimental and theoretical results. This section contains a description of the evolution of the universe as we understand it today, as illustrated by table 2.1. These results are fairly robust unless otherwise specified. This description of the evolution of the universe is called  $\Lambda$ -Cold Dark Matter (or  $\Lambda$ CDM for short) and has recently become predominant due to good experimental support.

### 2.1 The Big Bang

The universe started out some 14 billion years ago by being extremely dense and hot. Note however that we do not know what happened at the actual beginning, but we can extrapolate the current expansion of the universe back *towards* that time, which I call  $t_0 = 0$ . According to recent measurements, Spergel et al. (2003), this was  $13.7 \pm 0.2$  billion years ago.

Contrary to common belief, there was no "explosion", but merely a rapid expansion of the fabric of the universe, like the rubber of a balloon stretches when you inflate it. The expansion of the universe still continues today and there is no indication that the expansion has a center. In an infinite universe, the Big Bang occurred everywhere at once. How we can conceive an infinite energy density at  $t = 0$  or for that matter an infinite universe is a philosophical question. Physicists generally content themselves with starting the exploration a fraction of time after  $t = 0$ .

During this first (and extremely brief) period of the universe, all forces are believed to have been just one and the same. However, as the universe cooled off, the forces separated into the electric, magnetic, gravitational, and the weak and strong nuclear force. An analogy with this separation would be the melting of ice cubes in a glass, being separate objects below freezing but melting into one homogeneous water mass at higher temperatures.

Note that this unification of forces is a theory without direct experimental support. However, the subsequent evolution of the universe does not hinge on this unification.

### 2.2 Inflation

When the universe was roughly  $10^{-34}$  seconds old, a period of intensive expansion occurred and the universe became  $\sim 10^{50}$  times bigger in a fraction of a second. This expansion is called inflation.

This theory has some more experimental support than that of the unification of forces. In fact, it was introduced to alleviate three serious deficits of the Big Bang theory: the horizon, the flatness and

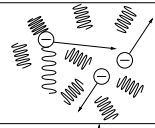
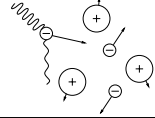
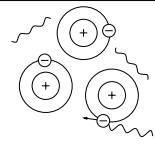
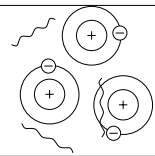
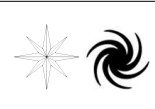
Time after BB	Events	Illustration
$\sim 10^{-43}$ s	Unification of forces?	
$\gtrsim 10^{-34}$ s	Inflation Exponential expansion	
$\gtrsim 10^{-10}$ s	Radiation domination Protons and neutrons are stable Antimatter disappears	
$\gtrsim 10^2$ s	Matter domination Hydrogen becomes stable Nucleosynthesis	
$\gtrsim 3 \times 10^5$ yrs	Decoupling of matter Transparent universe The Cosmic Microwave Background is released	
$\sim 10^9$ yrs	Structure formation The first stars and galaxies	

Table 2.1: History of the universe.



the monopole problem. Here comes a brief explanation of them. For more detail, I suggest Peacock (1998). The horizon problem stems from the measured correlation between parts of the universe that never have been in contact (due to the finite speed of light). The flatness problem is that the universe can be measured to be nearly flat, as far as we can see, and this is unlikely from a theoretical point of view. The monopole problem is about the absence of so called magnetic monopoles, which are theoretically predicted as a consequence of the unification of forces.

Furthermore, inflation also provides natural seeds for star and galaxy formation, through the growth of tiny quantum fluctuations into macroscopic fluctuations.

Although inflation has many attractive features, it is not yet a proved theory because many of the details still do not work out right in realistic calculations without assumptions that are poorly justified. Probably most cosmologists today believe inflation to be correct at least in its outlines, but further investigation will be required to establish whether this is indeed so.

## 2.3 Radiation Dominated Era

After approximately  $10^{-10}$  seconds the inflation period was at an end. The following epoch is called the radiation dominated era in which the principal component of the universe was radiation – photons.

During this era, the *antimatter* disappears from the universe through contact with matter and subsequent annihilation. However, due to a slight excess of matter over antimatter, the antimatter was all consumed and only the excess of ordinary matter remained.

The universe had also become cool enough to allow protons and neutrons to form and become stable (before this time, the quarks and gluons possibly co-existed in some sort of plasma). The protons are nothing but ionized hydrogen, which was the first type of atoms to form.

This early formation of particles touches upon the subject of particle physics in which the author has a particular interest. For more information about other possible types of particles, see Elfgren (2002a) and Elfgren (2002b).

## 2.4 Matter Dominated Era

Around one minute after the Big Bang, the radiation had lost enough energy density due to the expansion to allow matter to start dominating. This in turn, means that the expansion rate of the universe changed.

During the matter dominated era, the thermal energy became low enough to allow the ionized hydrogen atoms to capture and keep electrons, thus forming the first neutral atoms. Furthermore, protons and neutrons started to fuse to form helium and other heavier elements. This process is called the *Big Bang Nucleosynthesis* (BBN) but did last for only about three minutes, Alpher et al. (1948). After that time, the density and the temperature of the universe dropped below what is required for nuclear fusion (neutron capture). The brevity of BBN is important because it prevented elements heavier than beryllium from forming, while allowing unburned light elements, such as deuterium, to exist. The result of the BBN is that the universe contains 75% hydrogen, 25 % helium, 1% deuterium and small amounts of lithium and beryllium. This predicted distribution corresponds very well with the measured abundances. For more detail on the BBN, see e. g. Burles et al. (2001).

The matter dominated era extended until the dark energy took over after roughly five billion years.

## 2.5 Decoupling of Matter

When the temperature of the universe dropped below  $T \sim 0.25 \text{ eV} \sim 3000 \text{ K}$  the photons no longer had enough energy to ionize or excite the atoms. This means that the photons could neither lose, nor gain energy. Thus, the universe became transparent and the photons kept their energy indefinitely (unless otherwise perturbed). These photons are called the Cosmic Microwave Background (CMB) and their properties will be described in more detail in chapter 3.

In order to estimate this transition temperature, we calculate the temperature at which there is one exciting photon per proton. For a photon to excite a hydrogen atom, it needs at least  $E = 10.2 \text{ eV}$ , which corresponds to a transition from the ground state to the first excited state. This means that we require:

$$N_p = N_\gamma(E_\gamma > 10.2 \text{ eV}) = N_\gamma \cdot \frac{1}{e^{10.2 \text{ eV}/k_B T} - 1}, \quad (2.1)$$

where  $N_p$  and  $N_\gamma$  are the number densities of protons and photons respectively,  $k_B$  is Boltzmann's constant and  $T$  is the temperature of the photons. Using  $N_\gamma \sim 10^9 N_p$ , the temperature can be calculated to  $T \approx 5700 \text{ K}$ . If a more detailed calculation is made, the temperature is found to be approximately  $3000 \text{ K}$ , which corresponds to  $t \approx 300,000$  years after the Big Bang ( $z \sim 1100$ ). As the universe expands, this temperature decreases as  $1/R$  where  $R$  is the expansion factor ( $= 1/(1+z)$ ). Since the universe has expanded by a factor of 1100 since decoupling, the temperature of the CMB has now dropped to  $2.725 \text{ K}$ .

Obviously, this transition is not something that happened at one single time, but rather took something like 50,000 years ( $\Delta z \approx 100$ ).

## 2.6 Structure Formation

After the decoupling, the universe went through a period called the Dark Ages which lasted until the onset of star formation about a billion years later. During this epoch the only thing that happened is that the CMB propagated and the matter slowly contracted due to gravity. Regions in space with an initial over-density (created by the inflation) attracted more matter, and eventually the matter density became high enough to sustain fusion and thus the first generation of stars formed.

During the Dark Ages, dark matter played a key roll in shepherding matter into dense regions thus allowing star formation. The dark matter is described briefly in section 4.2.

## 2.7 The First Generation of Stars

The first stars are called population III stars due to properties that are rather different from those of the stars today. They are born in loosely bound gravitational structures defined by high baryon densities and a surrounding dark matter halo.

The source material of these stars is the matter that was created during the Big Bang nucleosynthesis, see section 2.4. This means that there is basically only hydrogen and helium in these stars. As time passed on, the source material for new stars had more and more heavy elements since the heavy elements were produced by the stars. The mass fraction of elements heavier than helium is called *metallicity*.

It is also believed that these first stars would have been rather heavy, see Cen (2003) and Fang and Cen (2004). The mass of the stars is characterized by the Initial Mass Function (IMF). With a low metallicity and a high mass, the stars will be short-lived and hot, Shioya et al. (2002). If the stars were not heavy, they would live longer and take more time to produce dust, thereby delaying the reionization to an improbable period.

## 2.8 Reionization

From decoupling until the reionization, the universe was made up of neutral atoms (along with photons, dark matter and dark energy).

At the onset of the first generation of stars, energetic photons were produced. This happened when  $z \sim 10$  and thus the CMB temperature was only  $T_{CMB} \sim 30$  K, while the star temperature could be over 80,000 K, see Shioya et al. (2002). At this temperature, the maximum emitted energy was at  $E_\gamma \sim 21$  eV, which was more than enough to ionize hydrogen ( $E_{H,ion} = 13.61$  eV). At the end of the intensive star formation period some five billion years after the Big Bang the universe slowly neutralized again, leaving us with a layer of ionized gas from  $t \sim 10^9$  years –  $5 \times 10^9$  years ( $z \sim 20-5$ ).

The universe was ionized in bulbs around the stars, and these bulbs expanded and eventually covered the entire universe. Due to this ionization the universe was no longer as transparent as it was before. The free electrons scattered the photons through the Compton process and thereby changed their energy and direction. The degree of change is characterized by the opacity,  $\tau_e$ , which is defined through

$$e^{-\tau_e} = \text{Probability of a photon to pass through the ionized layer without being scattered.} \quad (2.2)$$

The effect of the reionization on the properties of the CMB is important and will be discussed in more detail in section 3.3.



## Chapter 3

# The Cosmic Microwave Background

As described in section 2.5, the Cosmic Microwave Background (CMB) is simply radiation – light – with a blackbody spectrum of temperature  $T_{CMB} = 2.725$  K (presently).

There are several aspects of the CMB that makes it a most important cosmological tool. In the words of Stephen Hawing “it is the discovery of the century, if not of all time”. It is currently the only experimental tool that allows us to probe anything further away than distant quasars, which are  $\sim 12.7$  billion light years away. The reionization was at its end by then and the first star generation had also passed, as well as the first structures in the universe. But the CMB has passed all this and been slightly affected by these events, which have left imprints in the spectral and spatial signature of the CMB.

Looking at the CMB, we see the universe largely as it has been in its infancy, when it was merely 300,000 years old (and we can even see some traces from beyond that time).

From the CMB we can determine the age of the universe and its expansion rate; how much of the total energy content that is made out of ordinary matter (*baryons*), dark matter and dark energy; what the matter distribution was 300,000 years after the Big Bang and also approximately the subsequent formation of structure, such as clusters of galaxies.

The CMB has an almost perfect blackbody spectrum. There are, however, small perturbations in the spectrum, called *anisotropies*. These have characteristic length scales, which correspond to angular scales for our measurements, and depend on what is causing the anisotropy.

The anisotropies can be divided into two categories; primary and secondary. The primary anisotropies occur at, or just before, decoupling, while the secondary anisotropies occur after this event. For a more exhaustive treatment of these anisotropies, the reader is referred to Tegmark (1996).

The measured brightness can be divided into several components:

$$B(\hat{r}, \nu) = B_{CMB} + B_{SZ} + B_{dust} + B_{free-free} + \dots, \quad (3.1)$$

where  $B_{CMB}$  is the intensity of the initial blackbody spectrum plus the primary anisotropies,  $B_{SZ}$  is the intensity due to the Sunyaev-Zel’dovich effect,  $B_{dust}$  is due to the dust contribution and  $B_{free-free}$  is the intensity due to the thermal *bremsstrahlung* from within our galaxy. In section 3.2 and 3.3 we will return to these and other effects and foregrounds and describe them in more detail. Now the CMB-part can be Taylor expanded around its blackbody temperature:

$$T(\hat{r}) = T_0 + \Delta T_{CMB}(\hat{r}) \quad (3.2)$$

which gives

$$B_{CMB}(\hat{r}, \nu) \approx B_{T_0}(\nu) + \Delta T_{CMB}(\hat{r}) \left. \frac{dB(\nu)}{dT} \right|_{T=T_0}. \quad (3.3)$$

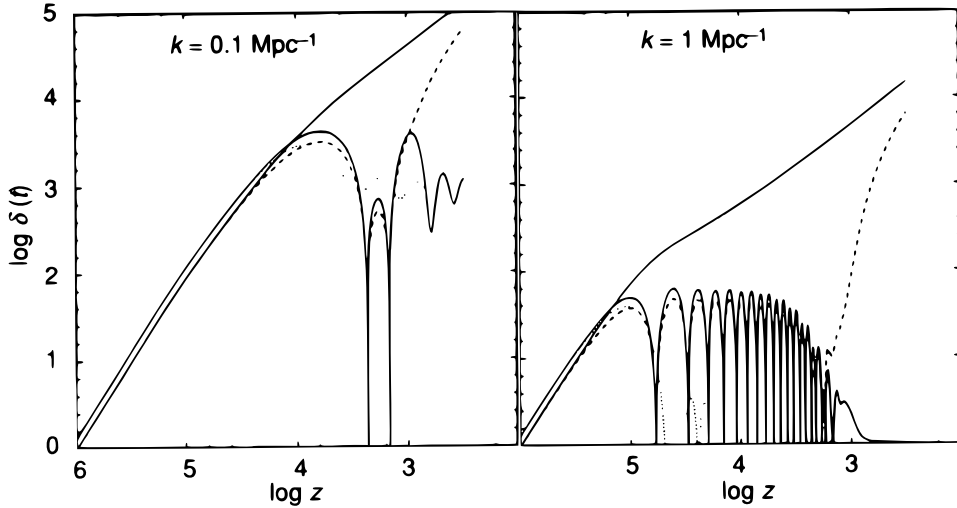


Figure 3.1: Illustration of Silk damping of an evolution of adiabatic perturbations in a cold dark matter model. Left panel: perturbations of co-moving scale 10 Mpc ( $\Leftrightarrow M \sim 10^{14} M_{\odot}$ ); right panel: perturbations of co-moving scale 1 Mpc ( $\Leftrightarrow M \sim 10^{11} M_{\odot}$ ). Reprinted from Peacock (1998).

The quantity measured by Planck (in the future) and many other instruments is only the relative excess over  $B_{T_0}$ , i. e. ,

$$\begin{aligned}
 \frac{B - B_{T_0}}{T_0(dB/dT)_{T_0}} &= \frac{\Delta T_{CMB}}{T_0} + \frac{B_{CMB} + B_{SZ} + B_{dust} + B_{free-free} + \dots}{T_0(dB/dT)_{T_0}} \\
 &\equiv \frac{\Delta T_{CMB}(v) + \Delta T_{SZ}(v, \hat{r}) + \Delta T_{dust}(v, \hat{r}) + \dots}{T_0}.
 \end{aligned} \tag{3.4}$$

The measured anisotropies consist of the  $\Delta T_X(v, \hat{r})/T_0$  terms in the expression above.

### 3.1 Primary Anisotropies

The primary anisotropies can be divided into three main categories: gravitational, adiabatic and Doppler. Other anisotropies, like topological defects, could also exist, but these are not considered to be very important and are beyond the scope of this introduction. The gravitational and adiabatic terms are combined on large angular scales ( $\gg 1$  degree) and are then called the Sachs-Wolfe effect, see Sachs and Wolfe (1967).

Furthermore, since the decoupling is not instantaneous, what we observe will be a weighted average over the thickness of the decoupling surface (also called the last scattering surface, LSS). This means that primary anisotropies smaller than this thickness ( $\Leftrightarrow \theta \sim 0.1^\circ$ ) will be washed out.

Another effect is the so called Silk damping, Silk (1968), which means that small matter perturbations will not survive, see figure 3.1. The reason for this damping is the fact that in small structures the photons will have time to diffuse out of the dense region before the end of decoupling. The typical mass scale of this effect is  $10^{11} M_{\odot}$ , the mass of an ordinary galaxy.

### 3.1.1 Gravitational Anisotropies

As the CMB photons climb out of a gravitational potential, they are redshifted by the gravity. In terms of an equivalent temperature this is given by

$$\left(\frac{\Delta T}{T}\right)_e = -\frac{\Delta\Phi_e}{c^2} \quad (3.5)$$

where  $\Delta\Phi_e$  is the gravitational potential in excess of the background.

### 3.1.2 Adiabatic Anisotropies

In a gravitational potential the number of photons is expected to be larger than normal and their temperature higher. At large angular scales ( $\gg 1$  degree), the induced anisotropies will be

$$\left(\frac{\Delta T}{T}\right)_e = \frac{2}{3} \frac{\Delta\Phi_e}{c^2}, \quad (3.6)$$

but on small scales, this is no longer the case due to *acoustic oscillations*.

This means that the Sachs-Wolf effect, which on large scales is the gravitational plus the adiabatic term, is

$$\left(\frac{\Delta T}{T}\right)_e = -\frac{1}{3} \frac{\Delta\Phi_e}{c^2}, \quad (3.7)$$

i. e. the photons are effectively redshifted by the gravitational potential. By measuring the size of these anisotropies and their relative strength we can estimate the matter distribution at the time of decoupling.

### 3.1.3 Doppler Anisotropies

Due to local movement of the plasma at the time of decoupling, there will be a kinetic Doppler shift

$$\left(\frac{\Delta T}{T}\right)_e = \frac{\vec{v}(\vec{r}) \cdot \hat{r}}{c}, \quad (3.8)$$

where  $\vec{v}(\vec{r})$  is the local velocity vector of the plasma at the point  $\vec{r}$ . This effect generally occurs at rather small scales compared to the Sachs-Wolf effect.

## 3.2 Secondary Anisotropies

The secondary anisotropies are effects that changed the CMB photons between decoupling and now. They can be divided into three types; gravitational effects, local ionization and global ionization. These will be described one by one below.

### 3.2.1 Gravitational Effects

There are three types of gravitational effects that affect the CMB; the early and the late integrated Sachs-Wolf effects, the Rees-Sciama effect and gravitational lensing.

The integrated Sachs-Wolf (ISW) effect comes into action when there is a change in a gravitational potential as a function of time:

$$\frac{\Delta T}{T} = \frac{\int \Delta\Phi(\vec{r}(t), t)}{c^2}, \quad (3.9)$$

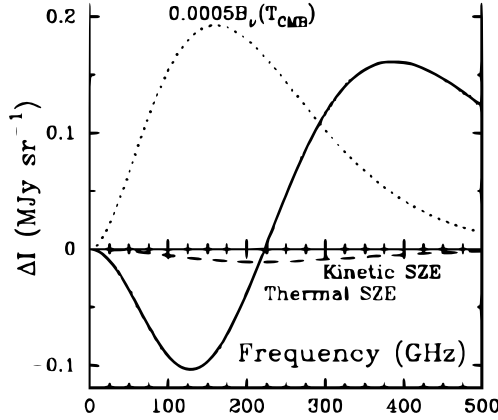


Figure 3.2: Illustration of the thermal and kinetic Sunyaev-Zel'dovich Effect (SZE). The graphs shows the intensity as a function of frequency. The thermal SZ effect increases the photons frequencies, through thermal excitation. The kinetic SZ effect decreases the intensity of the photons in this case because the gas cloud is moving from us.

where  $\Delta\Phi$  is the time derivative of the gravitational potential in excess of the background potential.

The *early ISW effect* is due to the fact that the photon contribution to the gravitational potential. Since the photon energy decreases with time, this will induce an integrated Sachs-Wolf effect.

The *late ISW effect* comes from the dark energy term that will become more and more important as time passes. This increase in energy also leads to an integrated Sachs-Wolf effect.

The Rees-Sciama effect is also called local ISW. It consists of galaxy clusters and other structures that evolve during the passage of the photons.

Gravitational lensing is an ISW effect perpendicular to the line of sight, affecting the angular distribution of the CMB and smearing it somewhat.

### 3.2.2 Local Reionization

The local reionization effect is when the reionization affects the CMB through the presence of ionized gas through which the CMB photons must pass. This effect comes about when energetic electrons hit the photons and transfer energy to the photons, and it is called inverse Compton scattering. The impact on the CMB of the inverse Compton scattering is called the Sunyaev-Zel'dovich (SZ) effect, Sunyaev and Zeldovich (1970), Sunyaev and Zeldovich (1980) and Rephaeli (1995). There are two types of the Sunyaev-Zel'dovich effect, thermal and kinetic, see figure 3.2.

The thermal SZ effect is due to energetic free electrons and will have the effect of shifting the CMB spectrum towards higher frequencies since each photon subject to the inverse Compton scattering will gain energy, but not in any particular direction.

The kinetic SZ effect is due to the global motion of a galaxy cluster or other large structures. Since there is a favored direction (in the direction of the velocity of the cluster), this will cause a Doppler shift of the CMB spectrum.

### 3.2.3 Global Reionization

There are three types of global reionization; suppression of small scales, new Doppler effect and the Vishniac effect.



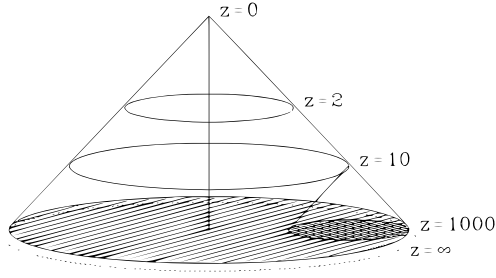


Figure 3.3: Illustration of the suppression of small scales due to the reionization. If photons scatter at reionization, they could come from anywhere within the lightcone projection at  $z = 1000$ . Through the finite speed of light, we know that they cannot have come from anywhere outside of this projection, which corresponds to an angle  $\sqrt{\Omega_0/z_i}$ .

The suppression of small scales comes from the fact that the photons scattering during reionization lose their original direction. The amplitude of this effect depends on the time when the reionization occurred, the later the higher amplitude, see figure 3.3. It also depends on the degree of reionization, in other words, on the *optical depth*. In fact, this effect suppresses all scales smaller than

$$\theta \leq \sqrt{\frac{\Omega_0}{z_i}}, \quad (3.10)$$

where  $\Omega_0$  is the total relative energy density of the universe and  $z_i$  is the *redshift* at reionization. The suppression of the *power spectrum* on these scales is  $e^{-2\tau}$ .

The new Doppler effect is due to local velocity and density perturbations, and the Vishniac effect is caused by electrons falling in gravitational potential wells, but it is only active on scales  $\theta \sim 0.02^\circ$  and even then it is quite feeble.

### 3.3 Foregrounds

Foregrounds are light sources in the universe emitting in the same frequency range as the CMB. There are three basic types of foregrounds; extragalactic, galactic and local.

#### 3.3.1 Extragalactic Foregrounds

The extragalactic foregrounds are point sources having an origin outside our galaxy. A point source has a very small angular extension. However, their total integrated effect can still be considerable. There are point sources that are active mostly in the radio domain, like e. g. radio galaxies, but there are also sources active mostly in the IR domain, like dusty galaxies.

As I have shown in my second paper, there is also a kind of continuous IR source all over the sky with a bias for mass concentrations – the emission from the early dust.

#### 3.3.2 Galactic Foregrounds

The galactic foregrounds are all diffuse, meaning that they have a certain angular extension. The principal galactic foregrounds are emission from dust, free-free emission and synchrotron radiation. The angular correlations, see section 3.4, of these foregrounds are all roughly  $\propto \theta^3$ .

The dust in our galaxy has been shown to have a Planck spectrum of temperature  $\sim 17$  K, Boulanger et al. (1996).

The free-free emission comes from free electrons that are accelerated, thus emitting thermal *bremsstrahlung*. The free-free emission is almost independent of frequency.

The synchrotron radiation is due to acceleration of plasmas and is a sort of global *bremsstrahlung*. The synchrotron radiation is most effective for frequencies below 70 GHz.

### 3.3.3 Local Foregrounds

Local foregrounds are perturbations from the solar system, like the planets, the moon, the Sun, the atmosphere and instrumental noise. The solar system perturbations are well known and the instrumental noise is instrument specific.

## 3.4 Power spectrum

In the previous section we saw that the measured anisotropies can be separated into several components, equation 3.4, each anisotropy with its specific spectral and spatial signature. In this section we will explore the *power spectrum*, which is a powerful tool to quantify the spatial signature of the signal.

The spatial signature is often expressed in terms of the Legendre spherical harmonics

$$\Delta T_X(\vec{r}, \nu) = \sum_{\ell=0}^{\infty} \sum_{m=-\ell}^{\ell} Y_{\ell m}(\vec{r}) a_{\ell m}^X(\nu), \quad (3.11)$$

where the spherical harmonics  $Y_{\ell m}$  are the basis functions and  $a_{\ell m}$  are their components. In order to determine correlations on different angular scales, the correlation functions are used:

$$C_{\ell}^X(\nu) = \frac{1}{2\ell + 1} \sum_{m=-\ell}^{\ell} \langle |a_{\ell m}^X(\nu)|^2 \rangle. \quad (3.12)$$

This is also called the (angular) power spectrum. In the case of isotropic fluctuations the above equation simplifies to  $\langle a_{\ell m}(\nu)^* a_{\ell' m'}(\nu) \rangle = \delta_{\ell\ell'} \delta_{mm'} C_{\ell}$ . To convert from  $\ell$  to  $\theta$  a good rule of thumb is  $\theta \approx 180^\circ / \ell$ .

It is customary to plot the quantity  $\ell(\ell + 1)C_{\ell}/2\pi$  in units of  $\mu\text{K}^2$ , cf figure 3.4. The reason for this choice is so that the root-mean-square (r.m.s.) of the temperature variations becomes visually apparent:

$$\langle \Delta T(\nu)^2 \rangle = \sum_{\ell=0}^{\infty} \left( \frac{2\ell + 1}{4\pi} \right) \approx \int_1^{\infty} \left( \frac{\ell(\ell + 1)}{2\pi} \right) C_{\ell} d(\ln \ell), \quad (3.13)$$

where we have used  $\frac{\ell(2\ell+1)}{4\pi} \approx \frac{\ell(\ell+1)}{2\pi}$  for  $\ell \gg 1$ . This means that in order to estimate the (r.m.s.)<sup>2</sup> of the anisotropies in the range  $\ell_1 < \ell < \ell_2$  we need to take only the r.m.s. height of the curve times  $\ln(\ell_2/\ell_1)$ .

### 3.4.1 Acoustic Oscillations

Prior to decoupling, the matter and the photons were tightly coupled and effectively formed a baryon-photon fluid. Because of the density perturbations, this fluid started to oscillate. These oscillations are called acoustic. Each mode in these oscillations will give rise to a correlation at a given angular scale in the power spectrum. The acoustic oscillations are a natural consequence of inflation and thus serves to corroborate the inflation theory.

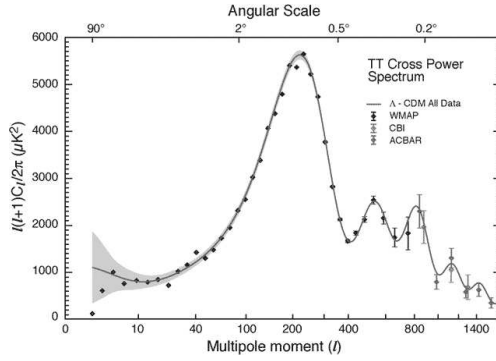
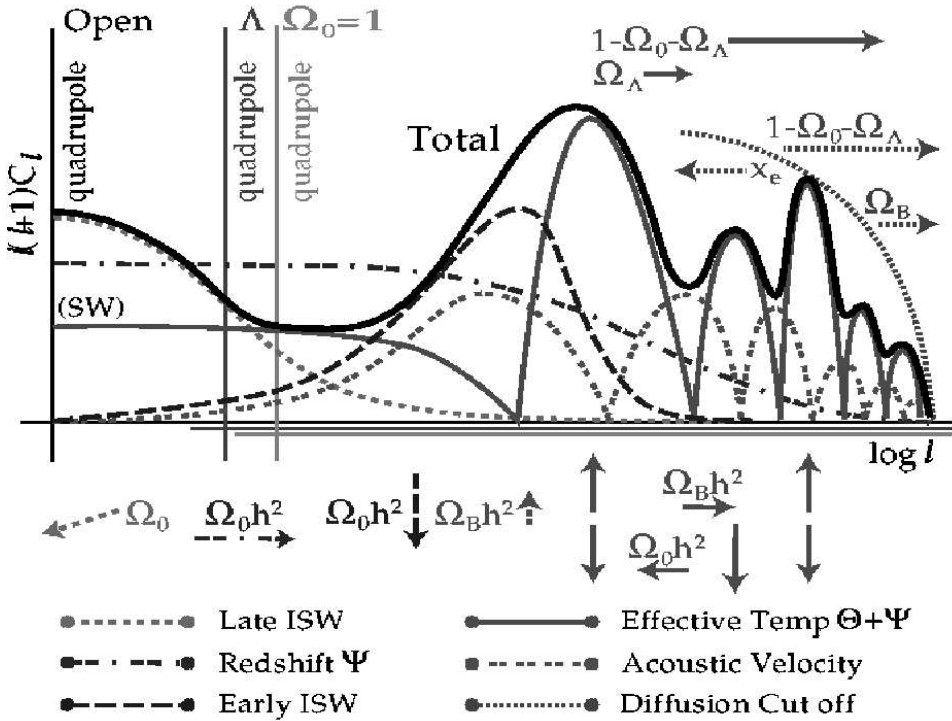


Figure 3.4: The power spectrum as measured by WMAP, CBI and ACBAR. On the x-axis, the inverse angular scale, on the y-axis, the correlation on that scale. The dots are data points and the curve is the theoretical curve.

### 3.4.2 Simulations of the CMB

A program named CMB-fast is used to estimate the CMB from theory. The program is versatile, allowing the user to test different scenarios with different types of cosmologies and see what the expected power spectrum would become. In figure 3.5 we can see the different components of the CMB and how they are affected by some cosmological parameters.



# Chapter 4

## Short Introduction to the Papers

This chapter is included to give the reader some background information that may be useful for the understanding of the particularities of the appended papers. Section 4.1 is describing the dust, which is the principal object of study in this thesis, and section 4.2 introduces dark matter, which is important for Paper II.

### 4.1 Dust

The abundance of dust in the universe can be calculated by estimating its production and destruction rate. These figures are not well known even of the nearby universe and even less so of the early universe. In this section the properties of this early dust are briefly discussed along with some general properties of the nearby dust. The section is included as a complement to my first paper, Elfgren and Désert (2004), where the specifics of early dust are used. For a more complete review of dust in general, see Draine (2003).

#### 4.1.1 Production

In section 2.4 we treated the formation of light elements through the nucleosynthesis, but most of the terrestrial material is made of heavier elements. The only known source of such heavy elements are *supernovæ*. During its life, a star fuses hydrogen into helium and then onto carbon, nitrogen and other heavy elements. If the star finishes as a supernova, these elements are released into the interstellar medium (ISM), and then serve to produce new planets and stars.

On their way out, many of these elements are ionized. When the ions meet they tend to form ionic bonds, and in this way tiny crystals are formed. These crystals form that we call cosmic dust.

For an overview of dust production in the early universe, the reader is referred to Todini and Ferrara (2001).

#### 4.1.2 Properties

The composition of interstellar dust grains is still largely unknown. While meteorites provide us with genuine specimens of interstellar grains for examination, these are subject to severe selection effects, and cannot be considered representative of interstellar grains. Our only direct information about the composition of interstellar dust comes from spectral features of extinction, scattering, or emission.

By means of spectral measurements and stellar nucleosynthesis it is found that dust grains are composed mainly of elements like silicon, oxygen, nitrogen, carbon and iron. Dust grains are formed of molecules like CO, SiO<sub>2</sub>, Al<sub>2</sub>O<sub>3</sub>, Fe, Fe<sub>3</sub>O<sub>4</sub>, MgSiO<sub>3</sub>, Mg<sub>2</sub>SiO<sub>4</sub> and amorphous carbon. These grains form at different temperatures. CO form at  $\approx 2500$  K (Fischer 2003), amorphous carbon at  $\approx 1800$  K, Al<sub>2</sub>O<sub>3</sub> at  $\approx 1600$  K and the other grain types at  $\approx 1100$  K (Todini and Ferrara 2001).

The polarization of starlight was discovered more than 50 years ago, and was immediately recognized as being due to aligned dust grains. Two separate alignments are involved: (1) alignment of the grain's principal axis of largest moment of inertia with its angular momentum  $J$ , and (2) alignment of  $J$  with the galactic magnetic field.

As has been shown by Woosley and Weaver (1995), the chemical composition can be found of different types of supernovæ with masses of 11-40  $M_{\odot}$  and metallicities  $Z/Z_{\odot} = 0, 10^{-4}, 0.01, 0.1$  and 1.

Galactic dust is found mostly in nebulae, where it is an important factor in the star formation process.

### 4.1.3 Destruction

The destruction of dust particles is not very well understood, due to the fact that the dust is found in a variety of environments of rather complicated nature. In this section, some important mechanisms for dust destruction are touched upon. Their exact impact, especially at the time of the early dust, remains unclear, see Draine (1990).

There are a number of phenomena that destroy dust (or rather erode it into negligible pieces). The destruction mechanisms include *sputtering* and grain-grain collisions in interstellar shocks, *sublimation* during supernovæ radiation pulses, sputtering and sublimation in H II regions, photodesorption by UV light and sputtering by cosmic rays. A classic paper on dust destruction is Draine and Salpeter (1979).

This plethora of processes makes it difficult to calculate the life time of the dust. For a hot ionized medium the lifetime can be estimated to  $10^8$  years, in a cold neutral medium, to  $10^9$  years and in a molecular cloud, to  $10^{10}$  years, Draine (1990). The actual environment of the dust from the first stars is pretty much unknown. What we do know, however, is that the universe was denser at that time than it is today, but also less clumped. There were no real galaxies, and in the beginning no ionized gas either.

## 4.2 Dark Matter

Dark Matter (DM) is not very well understood but there are several properties that are known. There are also a multitude of particles that could possibly constitute this mysterious DM. DM has not yet been directly seen neither in astronomical telescopes, nor in particle accelerators.

The DM was originally conceived to explain the velocities of stars in galaxies as a function of their distance from the center. For each of the stellar, galactic, and galaxy cluster/supercluster observation the basic principle is as follows. If we measure velocities in some region, there has to be enough mass present for gravity to stop all the objects flying apart. When such velocity measurements are done on large scales, it turns out that the amount of inferred mass is much more than can be explained by the luminous stuff. Hence we infer that there is DM in the Universe.

DM is also required in order to enable gravity to amplify the small fluctuations in the Cosmic Microwave Background enough to form the large-scale structures that we see in the universe today, as mentioned in section 2.6.

DM candidates are usually split into two broad categories, with the second category being further sub-divided:

- Baryonic
- Non-Baryonic
  - Hot Dark Matter (HDM) and
  - Cold Dark Matter (CDM),

depending on their respective masses and speeds. CDM candidates travel at slow speeds (hence "cold") or have little pressure, while HDM candidates move rapidly (hence "hot").

Since the DM has yet eluded detection, it is supposed that it will only interact very weakly with ordinary matter. This means that simulations of the structure evolution of the universe can be greatly simplified. Since we know that the gravitationally dominant form of matter in the early universe was DM, and its only interaction is gravitation, the equations of evolution are rather simple to solve. This means that huge simulations can be done including millions of DM particles and covering hundreds of Mpc (mega parsecs). In simulations each "particle" weighs in the order of  $10^{10}$  solar masses.





# Chapter 5

## Summary and Outlook

### 5.1 Summary

The universe truly is a marvelous place, and it is astonishing how much we can learn about its history and evolution just by observing some light that happens to fall on the surface of the Earth.

One of the things we might learn in the near future is the impact of dust from the first generation of stars. Since the dust will have a particular spatial and spectral signature it could very well be detected by the Planck satellite, planned to be launched in 2007.

This dust could help us better understand two important things in the universe, the Cosmic Microwave Background and the formation of structures like galaxies and stars in the early universe.

The evolution of the universe has been treated in chapter 2 in order to set the stage for the place of the dust in the history of the universe. The most important points were: (1) The decoupling of matter from radiation (section 2.5), leaving the universe with an omnipresent radiation with an imprint of the properties of universe when it was 300,000 years old; (2) The first generation of stars (section 2.7), which exploded as supernovæ and sprayed out heavy materials that condensed to form dust.

In chapter 3 follows a description of the properties and benefits of the Cosmic Microwave Background. This CMB radiation contains a wealth of cosmological information, which can be extracted with the help of the power spectrum (section 3.4).

Chapter 4 contains a description of our current knowledge of interstellar dust (section 4.1) and gives an introduction to dark matter (section 4.2). Neither of these subjects are particularly well known to us today, but there is a lot of circumstantial evidence that helps us understand the basics.

In the first appended paper, Elfgren and Désert (2004), a simple method is used to determine the dust density as a function of time. The ambient radiation from the first generation of stars will heat this dust and it will reemit a different spectrum. When this emission is integrated along the line of sight through all the dust, a unique spectrum is obtained that could be measured here on Earth. Unfortunately, the current generation of instruments are not capable of identifying the dust signal merely by using the dust spectrum.

In the second paper, Elfgren et al. (to be published), the spatial distribution of dust is the object of study. Since very little is known about this time in the history of the universe, a crude method for the density distribution of the dust is used. The method simply consists of letting the dust be proportional to the dark matter density, since dark matter is believed to have played a key-role in the evolution of large-scale structures like galaxy clusters. Through computer simulations of the evolution of dark matter, the distribution of the dust in space is thus obtained. The knowledge of the spatial distribution is then compared to the sensitivity of the planned Planck satellite. The results are promising but depend on model parameters like the lifetime of this early dust.

The goals of this Licentiate thesis, as presented in the Introduction, have thus been satisfyingly accomplished. The thickness, density and distribution of the dust from the first generation of stars have been estimated, and the impact of this dust on the CMB measurements has been evaluated.

## 5.2 Outlook

There are still numerous exciting problems to be solved in order to consolidate our understanding of the universe. In particular, the impact of dust on the history of the universe is still an open question. It would be interesting to see some detailed simulations of the evolution of the first galaxies, with dust production and destruction taken into account. This dust has important implications for the spectra emitted by these galaxies, which eventually could be detected, for example with the Hubble telescope. Hubble Ultra Deep Field observations have been carried out but are not yet published, and these observations should show us the universe at an age of 0.3-0.7 billion years. This would mean that we could even get a glimpse of the first generation of stars and find out some more direct evidence of their properties.

Aside from the implications of dust in the early universe, gravitation is still a hot subject. Our present understanding of what takes place with dynamics in the vicinity of a black hole is still poor, and there are other aspects of gravitation that are not fully understood either.

Another interesting path is to study the large scale structure of the universe. There are some tantalizing evidence that the universe might not be as isotropic and homogeneous as has been previously presumed.

New instruments are continuously being developed and our understanding of the universe is growing rapidly. All in all, the prospects of astrophysics are excellent in the future, and I look forward to take part in the exploration of it.

# Bibliography

- Alpher, R. A., Herman, R. and Gamow, G. A. (1948), ‘Thermonuclear Reactions in the Expanding Universe’, *Phys. Rev.* **74**, 1198–1199.
- Boulanger, F., Abergel, A., Bernard, J.-P., Burton, W. B., Desert, F.-X., Hartmann, D., Lagache, G. and Puget, J.-L. (1996), ‘The dust/gas correlation at high Galactic latitude.’, *A&A* **312**, 256–262.
- Burles, S., Nollett, K. M. and Turner, M. S. (2001), ‘What is the big-bang-nucleosynthesis prediction for the baryon density and how reliable is it?’, *Phys. Rev. D* **63**(6), 512–519.
- Cen, R. (2003), ‘The Implications of Wilkinson Microwave Anisotropy Probe Observations for Population III Star Formation Processes’, *ApJL* **591**, L5–L8.
- Draine, B. T. (1990), ‘Evolution of interstellar dust’, in ‘ASP Conf. Ser. 12: The Evolution of the Interstellar Medium’, pp. 193–205.
- Draine, B. T. (2003), ‘Astrophysics of Dust in Cold Clouds’, *ArXiv Astrophysics e-prints*, *astro-ph/0304488*, pp. 1–93.
- Draine, B. T. and Salpeter, E. E. (1979), ‘Destruction mechanisms for interstellar dust’, *ApJ* **231**, 438–455.
- Elfgren, E. (2002a), ‘Detection of a Hypercharge Axion in ATLAS’, in ‘Fundamental Interactions, Proceedings of the Sixteenth Lake Louise Winter Institute, held 18-24 February, 2001. Edited by A. Astbury, B. A. Campbell, F. C. Khanna, and M. G. Vincter. World Scientific Publishing Company, 2002., p.185’, pp. 185–192.
- Elfgren, E. (2002b), ‘Heavy and excited leptons in the opal detector?’, *ArXiv Astrophysics e-prints*, *hep-ph/0209238*, pp. 1–85.
- Elfgren, E. and Désert, F.-X. (2004), ‘Dust from reionization’, *A&A* **425**, 9–14.
- Elfgren, E., Désert, F.-X. and Guiderdoni, B. (to be published), ‘Dust distribution during reionization’, *submitted to A&A*, pp. 1–5.
- Fang, T. and Cen, R. (2004), ‘The Transition from Population III to Population II Stars’, *ApJL* **616**, L87–L90.
- Fischer, E. (2003), ‘Extinction by grey dust in the intergalactic medium’, *ArXiv Astrophysics e-prints*, *astro-ph/0306459*, pp. 1–6.
- Mather, J. C., Fixsen, D. J., Shafer, R. A., Mosier, C. and Wilkinson, D. T. (1999), ‘Calibrator Design for the COBE Far-Infrared Absolute Spectrophotometer (FIRAS)’, *ApJ* **512**, 511–520.

- Mohr, P. J. and Taylor, B. N. (2000), 'CODATA Recommended Values of the Fundamental Constants', in 'AIP Conf. Proc. 543: Atomic and Molecular Data and their Applications, ICAM-DATA', pp. 1–333.
- Peacock, J. (1998), *Cosmological Physics*, Cambridge University Press, Cambridge, U.K.; New York, U.S.A.
- Rephaeli, Y. (1995), 'Comptonization Of The Cosmic Microwave Background: The Sunyaev-Zeldovich Effect', *ARA&A* **33**, 541–580.
- Sachs, R. K. and Wolfe, A. M. (1967), 'Perturbations of a Cosmological Model and Angular Variations of the Microwave Background', *ApJ* **147**, 73–90.
- Schaller, G., Schaerer, D., Meynet, G. and Maeder, A. (1992), 'New grids of stellar models from 0.8 to 120 solar masses at  $Z = 0.020$  and  $Z = 0.001$ ', *A&AS* **96**, 269–331.
- Shioya, Y., Taniguchi, Y., Murayama, T., Nishiura, S., Nagao, T. and Kakazu, Y. (2002), 'Effects of a Burst of Formation of First-Generation Stars on the Evolution of Galaxies', *ApJ* **576**, 36–44.
- Silk, J. (1968), 'Cosmic Black-Body Radiation and Galaxy Formation', *ApJ* **151**, 459–471.
- Spergel, D. N., Verde, L., Peiris, H. V., Komatsu, E., Nolta, M. R., Bennett, C. L., Halpern, M., Hinshaw, G., Jarosik, N., Kogut, A., Limon, M., Meyer, S. S., Page, L., Tucker, G. S., Weiland, J. L., Wollack, E. and Wright, E. L. (2003), 'First-Year Wilkinson Microwave Anisotropy Probe (WMAP) Observations: Determination of Cosmological Parameters', *ApJS* **148**, 175–194.
- Sunyaev, R. A. and Zeldovich, I. B. (1970), 'Small-Scale Fluctuations of Relic Radiation', *Ap&SS* **7**, 3–19.
- Sunyaev, R. A. and Zeldovich, I. B. (1980), 'Microwave background radiation as a probe of the contemporary structure and history of the universe', *ARA&A* **18**, 537–560.
- Tegmark, M. (1996), 'Doppler Peaks and all that: CMB Anisotropies and What They Can Tell Us', in S. Bonometto, J. R. Primack and A. Provenzale, eds, 'Dark Matter in the Universe, Proc. of the Int. School of Physics Course CXXXII', Italian Physical Society, Oxford, GB: IOS Press, pp. 379–419.
- Todini, P. and Ferrara, A. (2001), 'Dust formation in primordial Type II supernovae', *MNRAS* **325**, 726–736.
- Woosley, S. E. and Weaver, T. A. (1995), 'The Evolution and Explosion of Massive Stars. II. Explosive Hydrodynamics and Nucleosynthesis', *ApJS* **101**, 181–235.

# Appendix A

## Cosmology

### A.1 Basic Introduction

This appendix contains some explanations for those not so familiar with cosmology but with some knowledge of physics in general. The symbols are explained in appendix B.

First, it is important to know that distance and time are used interchangeably. Since light moves with a constant speed,  $c$ , we know that the distance travelled will be  $c \cdot t$ . So, if we say that something is 100 light years away this means that it was 100 years ago.

Another important measure of distance is (cosmological) redshift,  $z$ . The relation between time,  $t$ , and redshift,  $z$ , is given in section A.2 and is also plotted in figure A.1. Astronomers and astrophysicists often mean distance when they speak about redshift, cosmologists often mean time.

In fact, the definition of redshift is:

$$z = \frac{\lambda_0 - \lambda_e}{\lambda_e} \quad (\text{A.1})$$

where  $\lambda_0$  is the observed wavelength and  $\lambda_e$  is the emitted wavelength. The reason why  $\lambda_0 \neq \lambda_e$  is the expansion of the universe – the light waves also expand and thus their wavelength increases. Consequently the redshift can also be expressed as  $z + 1 = 1/R$ , where  $R$  is the expansion of the universe. Note that light emitted nearby will not have been subject to any expansion of the universe and thus is at  $z = 0$ .

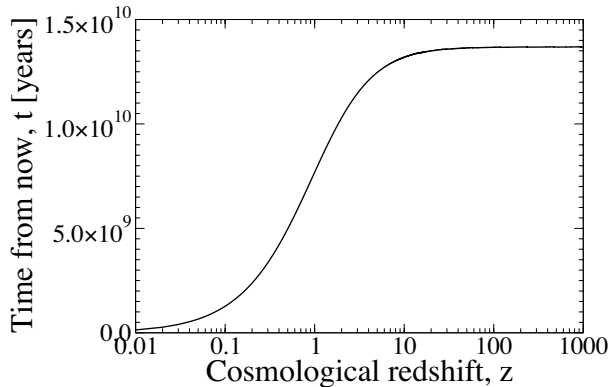


Figure A.1: Time versus redshift.

## A.2 Cosmological Equations

Relation between temperature,  $T$ , expansion of the universe  $R$  and time since the Big Bang,  $t$ :

Radiation dominated universe:

$$T \propto 1/R \propto 1/t^{1/2}. \quad (\text{A.2})$$

Matter dominated universe:

$$T \propto 1/R \propto 1/t^{2/3}. \quad (\text{A.3})$$

Evolution of matter and radiation density:

Matter density:

$$\rho_M \propto R^{-3}. \quad (\text{A.4})$$

Radiation density:

$$\rho_R = \sigma T^4 / c^2 \propto R^{-4}. \quad (\text{A.5})$$

General:

Time/redshift (for  $z < 1000$ ):

$$\frac{dz}{dt} = -H_0 \sqrt{(1+z)^2(1 - \Omega_m + \Omega_m(1+z)^3)}. \quad (\text{A.6})$$

Measured angles:

$$\frac{\pi}{\ell} \approx \theta[\text{rad}] = \frac{D_c}{L_c} = \frac{D_c}{c \cdot \int_{t_i}^{t_0} (1+z) dt} = \frac{D_c}{c \int_z^0 dz(1+z) \frac{dt}{dz}}, \quad (\text{A.7})$$

where  $D_c$  denotes the co-moving distance and the other symbols are explained in appendix B.

Spectra:

Blackbody spectrum:

$$B_\nu = \frac{2h\nu^3}{c^2} (e^{h\nu/k_B T} - 1)^{-1}. \quad (\text{A.8})$$

Conversion  $\nu \leftrightarrow \lambda$ :

$$f(\nu)d\nu = f(\lambda)d\lambda, \quad \forall f. \quad (\text{A.9})$$

# Appendix B

## Explanations

### B.1 Glossary

For further descriptions of astronomical terms, the interested reader is referred to <http://factguru.com/>.

**Acoustic oscillations** The oscillations due to density variations in the photon-baryon fluid prior to decoupling.

**Antimatter** Antimatter is constituted of *antiparticles*.

**Antiparticle** An antiparticle is defined as having the opposite *quantum numbers* of the corresponding particle, but it has the same mass.

**Baryonic matter** “Ordinary matter” consisting of baryons, i. e. protons and neutrons.

**Big Bang** The origin of the universe - see section 2.1.

**Bremsstrahlung** Radiation emitted due to acceleration of charged particles.

**CMB** Cosmic Microwave Background. The fossil radiation left from the *decoupling* of radiation from matter,  $\sim 300,000$  years after the *Big Bang*. The CMB radiation has a blackbody spectrum with a temperature of  $T_{CMB} = 2.725 \pm 0.002$  K, Mather et al. (1999).

**Dark Matter** Exotic dark matter is believed to constitute  $\sim 25\%$  of the total mass (energy) of the universe. Ordinary (*baryonic*) matter only constitutes  $\sim 5\%$  of the total mass (energy) of the universe. The domination of dark matter is inferred from the rotations of galaxies and the evolution of large scale structures (e. g. galaxy clusters) in the universe. Note, however, that ordinary matter invisible to us also is dark matter. It is still and unsettled question, what dark matter actually is. For more information, see section 4.2.

**Decoupling** When there was not enough thermal energy to excite hydrogen, the energy of the photons did not change anymore and they continued virtually unhindered.

**Early ISW effect** This is due to the fact that the photons contribute to the gravitational potential. Since the photon energy decreases with time, this will induce an integrated Sachs-Wolf effect.

**Foregrounds** Other signals that (partly) hide the primordial CMB. Examples: Our galaxy and point sources like nearby planets and distant galaxies and dust, cf section 3.3.

**GalICS** A computer program used to simulate dark matter and the evolution of galaxies and their spectra.

**Integrated Sachs-Wolf effect** When a gravity potential changes over time. See section 3.2.

**Late ISW effect** This comes from the dark energy term that will become more and more important as time passes. This increase in energy also leads to an integrated Sachs-Wolf effect.

**Metallicity** The mass proportion of elements heavier than helium, denoted  $Z$ . The Sun has a metallicity of  $Z_{\odot} \approx 0.02$ , Schaller et al. (1992).

**Optical depth,  $\tau$**  The probability of a photon passing through a medium without scattering is  $e^{-\tau}$ .

**Planck** A satellite, which will be launched in 2007 and which is planned to measure the CMB over the entire sky with unprecedented precision.

**Population III stars** The first generation of stars with extremely low *metallicity* and probably a high mass and a short life.

**Power spectrum** A plot of the angular correlations of the measured CMB, cf section 3.4.

**Quantum numbers** The numbers, which can be said best to describe the state of a particle. Examples: electric charge ( $Q$ ), lepton number ( $L$ ), baryon number ( $B$ ), parity ( $P$ ), spin ( $S$ ), isospin ( $I$ ), strangeness ( $S$ ), and charge conjugation ( $C$ ).

**Quasar** Extremely distant and luminous astronomical objects, which are much smaller than a galaxy and much more luminous.

**Redshift** Used to measure distance from us to a source (a star, a galaxy etc). Equivalently redshift measures time from now and backwards. Today the universe has  $z = 0$ . A billion years ago correspond to  $z \sim 0.1$ , ten billion years ago to  $z \sim 2$ , thirteen billion years ago to  $z \sim 8$ . The redshift is due to the expansion of the Universe. Contrary to popular belief, this is not a Doppler shift. Most galaxies move away from us, but this is not the cause of their redshifts. Instead, as a light wave travels through the fabric of space, the universe expands and the light wave gets stretched and therefore redshifted. See also appendix A.

**Reionization** This happened when the first generation of stars formed, emitting high energy photons capable of ionizing the hydrogen and helium gas. The reionization lasted for some five billion years.

**Sachs-Wolf effect** When a photon has to climb out of a gravity well and thereby gets redshifted.

**Silk damping** Damping of density perturbations up to  $10^{11} M_{\odot}$  prior to *decoupling*, due to photon diffusion.

**Sputtering** Bombarding a target material with energetic (charged) atoms, which release atoms from the target, thus eroding it.

**Sublimation** The change of a solid substance directly into a vapor without first passing through the liquid state.

**Sunyaev-Zel'dovich effect** When an electron hits a photon and gives it energy. See section 3.2.

**Supernova** A gigantic stellar explosion in which the luminosity of the star suddenly increases by as much as a billion times. Most of its substance is blown off, leaving behind, at least in some cases, an extremely dense core, which may become a neutron star.



## B.2 Abbreviations

BBN	Big Bang Nucleosynthesis
CDM	Cold Dark Matter
CMB	Cosmic Microwave Background
DM	Dark Matter
GalICS	Galaxies In Cosmological Simulations
HDM	Hot Dark Matter
IGM	InterGalactic Medium
ISM	InterStellar Medium
ISW	Integrated Sachs-Wolf effect
PAH	Polycyclic Aromatic Hydrocarbon
SN	SuperNova
SZ	Sunyaev-Zel'dovich effect
WMAP	Wilkinson's Microwave Anisotropy Probe

## B.3 List of Variables

$B(\hat{r}, \nu)$	Measured intensity in $\text{W}/\text{m}^2$ in direction $\hat{r}$ .
$B_X = B_X(\hat{r}, \nu)$	Intensity of component $X$ .
$\Delta\Phi$	Gravitational potential excess over background.
$z$	The <i>redshift</i> , which is dimensionless, is often used to describe time or length through the intermediary of the expansion of the universe $R$ . See also figure A.1.
$R$	The expansion of the universe is $\propto R$ , see $z$ .
$T$	Temperature in Kelvin.
$t$	Time in seconds.
$\theta$	Angle on the sky.
$N_p$	Number density of protons.
$N_\gamma$	Number density of photons.
$E_\gamma$	Energy of photons.
$z_i$	Redshift of the reionization.
$\vec{r}$	Spatial coordinate vector.
$\vec{v}$	Velocity vector.
$\Delta T_X$	Anisotropy for component $X$ .
$\ell$	Inverse angle scale, $\theta \approx 180^\circ/\ell$ .
$C_\ell$	Angular correlation on scale $\ell$ .
$\nu$	Frequency in Hz.
$Y_{\ell m}(\theta, \phi)$	Angular basis function for the Legendre spherical harmonics.
$a_{\ell m}$	Component of $Y_{\ell m}$ .
$\sqrt{\langle \Delta T(\nu)^2 \rangle}$	Root mean square of temperature differences.

## B.4 List of Cosmological Constants

$h_0$	$0.72 \pm 0.03$	Hubble's relative constant (Spergel et al. 2003).
$H_0 = 100 \cdot h_0 \frac{\text{km/s}}{\text{Mpc}}$	$2.33 \times 10^{-18} \text{s}^{-1}$	Hubble's constant.
$\rho_c = \frac{3H_0^2}{8\pi G}$	$(0.97 \pm 0.04) \times 10^{-26} \text{kg/m}^3$	Critical density of the universe
$\Omega_{tot} = \rho_{tot}/\rho_c$	$1.02 \pm 0.02$	Total relative energy content of the universe, (Spergel et al. 2003).
$\Omega_m = \rho_m/\rho_c$	$(0.133 \pm 0.006)/h^2$	Relative matter content of the universe, (Spergel et al. 2003).
$\Omega_b = \rho_b/\rho_c$	$(0.0226 \pm 0.0008)/h^2$	Relative baryon content of the universe, (Spergel et al. 2003).
$M_\odot$	$1.99 \times 10^{30} \text{kg}$	Mass of the Sun.

## B.5 List of Physical Constants and Units

$c$	299792458 m/s	Speed of light in vacuum, from Latin "celeritas"=speed.
$G$	$6.6742(10) \times 10^{-11} \text{m}^3/\text{kg}\cdot\text{s}^2$	Newton's constant of gravitation (Mohr and Taylor 2000).
$k_B$	$1.3806505 \times 10^{-23} \text{J/K}$	Boltzmann's constant.
1 erg	$10^{-7} \text{J}$	Unit energy in the cgs (centimeter-gram-second) system of units.
1 eV	$1.602 \times 10^{-19} \text{J}$	Electron volt, energy.
1 pc	$3.086 \times 10^{16} \text{m}$	A parsec is defined as the distance from the Sun which would result in a parallax of 1 second of arc as seen from Earth,.

## **Appendix C**

# **Appended Papers**



---

# Paper I

---

## **Dust from Reionization**

The production of dust in the early universe is estimated from the number of stars needed to achieve reionization. The spectral signature of the dust is calculated and compared to measurements. The contribution from the dust layer to the Cosmic Microwave Background is found to be small.

Elfgren, Erik and Désert, François-Xavier, 2004, *Astronomy and Astrophysics*, **425**, 9-14.



## Dust from reionization

E. Elfgrén<sup>1</sup> and F.-X. Désert<sup>2</sup>

<sup>1</sup> Department of Physics, Luleå University of Technology, 971 87 Luleå, Sweden  
 e-mail: elf@ludd.luth.se

<sup>2</sup> Laboratoire d'Astrophysique, Observatoire de Grenoble, BP 53, 414 rue de la piscine, 38041 Grenoble Cedex 9, France

Received 6 October 2003 / Accepted 13 May 2004

**Abstract.** The possibility that population III stars have reionized the Universe at redshifts greater than 6 has recently gained momentum with WMAP polarization results. Here we analyse the role of early dust produced by these stars and ejected into the intergalactic medium. We show that this dust, heated by the radiation from the same population III stars, produces a submillimetre excess. The electromagnetic spectrum of this excess could account for a significant fraction of the FIRAS (Far Infrared Absolute Spectrophotometer) cosmic far infrared background above 700 micron. This spectrum, a primary anisotropy ( $\Delta T$ ) spectrum times the  $\nu^2$  dust emissivity law, peaking in the submillimetre domain around 750 micron, is generic and does not depend on other detailed dust properties. Arcminute-scale anisotropies, coming from inhomogeneities in this early dust, could be detected by future submillimetre experiments such as Planck HFI.

**Key words.** cosmology: cosmic microwave background – cosmology: early Universe

### 1. Introduction

More accurate measurements of the cosmic microwave background (CMB) implies a need for a better understanding of the different foregrounds. We study the impact of dust in the very early universe  $5 < z < 15$ . WMAP data on the CMB polarization, Kogut et al. (2003) provides a strong evidence for a rather large Thomson opacity during the reionization of the Universe:  $\tau_e = 0.17 \pm 0.04$  (68% C.L.). Although the mechanism of producing such an opacity is not fully understood, Cen (2002, 2003) has shown that early, massive population-III (Pop III) stars could ionize the Universe within  $5 < z < 15$  (see Figs. 1 and 2). Adopting this hypothesis, we discuss the role and observability of the dust that is produced by the Pop III stars. As we can only conjecture about the physical properties and the abundance of this early dust, we adopt a simple dust grain model with parameters deduced from the Milky Way situation. The dust production is simply linked to the ionizing photon production by the stars through their thermal nuclear reactions. The low potential well of the small pre-galactic halos allows the ejected dust to be widely spread in the intergalactic medium. The ionizing and visible photons from the same Pop III stars heat this dust. There are no direct measurements of this dust, but by means of other results the amount of dust can be estimated. A similar study has been done for a later epoch of the universe, in which data are more readily available, Pei et al. (1999). We use a cosmology with  $\Omega_{\text{tot}} = \Omega_m + \Omega_\Lambda = 1$ , where  $\Omega_m = \Omega_b + \Omega_{\text{DM}} = 0.133/h^2$ ,  $\Omega_b = 0.0226/h^2$  and  $h = 0.72$  as advocated by WMAP, Spergel et al. (2003), using WMAP data in combination with large scale structure

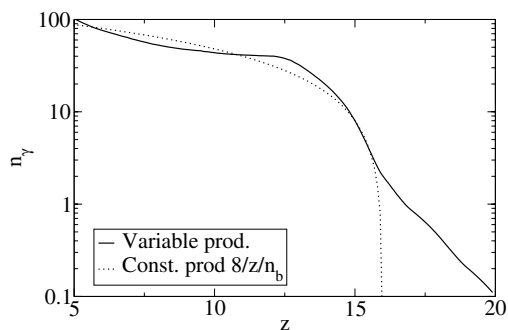


**Fig. 1.** Total number of ionizing photons produced from Pop III stars per baryon, cf. (Cen 2002, Fig. 14). The dotted line represents a simplified model with a constant photon production, from  $z = 16$ , of 8 per unit  $z$  per baryon. The results are similar.

observations (2dFGRS + Lyman  $\alpha$ ). Furthermore, since  $z \gg 1$  the universe is matter-dominated. We relate all cosmological parameters to their measurement today so that they have their present-day values throughout our calculations.

We now proceed to compute the abundance and the temperature of this dust. Consequences on the CMB distortions are then to be discussed.

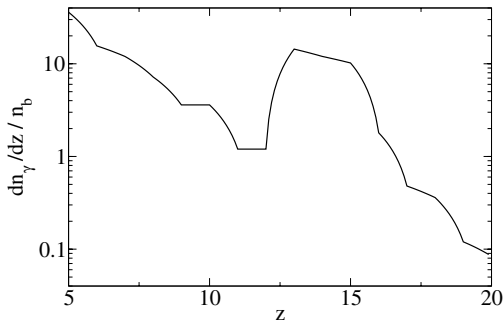


**Fig. 2.** Production rate of ionizing photons from Pop III stars per baryon,  $\frac{dn_\gamma}{dz}/n_b$ . The odd form between each integer  $z$  is not physical but are due to the fact that the redshift  $z$  is a nonlinear function of time.

## 2. Dust model

Here we assume the dust properties to be similar to what is observed in our galaxy. For simplicity, we suppose spherical dust grains with radius  $a = 0.1 \mu\text{m}$  and density  $\rho_g = 2.3 \times 10^3 \text{ kg/m}^3$ . The absorption cross section,  $\sigma_\nu$ , between photons and dust can be written as

$$\sigma_\nu = Q_\nu \pi a^2, \quad (1)$$

where we parametrize the frequency dependency as

$$Q_\nu = \begin{cases} Q_0 \frac{a}{a_r} \left(\frac{\nu}{\nu_r}\right)^{\beta_\nu} & \text{submm and infra red (IR),} \\ 1 & \text{visible and ultra violet (UV),} \end{cases} \quad (2)$$

where  $\nu_r$ ,  $a_r$  and  $Q_0$  are normalization constants. There is only one independent constant which means that we can fix  $a_r = 0.1 \mu\text{m}$ . In (Desert et al. 1990, Fig. 3) the poorly known knee wavelength,  $\lambda_r = c/\nu_r$  was set to  $100 \mu\text{m}$ . Here, we choose  $40 \mu\text{m}$  for simplicity, so that early dust radiates mostly in the  $\nu^2$  emissivity regime. Above the characteristic frequency  $\nu_r$ , the spectral index  $\beta = 1$ , below  $\beta = 2$ . The exact position of  $\nu_r$  is not very important for our study because it is mainly above the interesting wave-length region  $\sim 0.3\text{--}3 \text{ mm}$  and it will not change the magnitude of the signal.

In the submm and far IR range, the spectral index is constant, and with  $Q_0 = 0.0088$  the assumed opacity agrees well with measurements by FIRAS on cirrus clouds in our galaxy, cf. Boulanger et al. (1996); Fixsen et al. (1998); Lagache et al. (1999). In the visible and UV region, the cross section is independent of the frequency because  $\lambda < 2\pi a$ . In the submm region, the cross section is proportional to the mass of the grain.

In order to evaluate the significance of the dust during the reionization, we calculate the amount of dust present in the universe at a given time. The co-moving relative dust density is  $\Omega_{d,0} = \rho_d(z)/(1+z)^3 \rho_c$ , where  $\rho_d(z)$  is the dust density,  $z$  is the red-shift,  $\rho_c = \frac{3H_0^2}{8\pi G}$  is the critical density ( $H_0$  and  $G$  are Hubble's and Newton's constants, respectively). The co-moving relative dust density as measured today evolves as:

$$\frac{d\Omega_{d,0}}{dz} = J_+ - J_-, \quad (3)$$

where  $J_+$  and  $J_-$  are the production and the destruction rate respectively.

The Pop III stars produce enough photons for the reionization while burning H and thus forming metals (Li and higher). These metals are released in supernovae explosions at the end of the stars short lives ( $\sim 1 \text{ Myr}$ ), whereafter they clump together to form dust, Nozawa et al. (2003). Knowing the production rate of ionizing photons to be  $\frac{dn_\gamma}{dz}/n_b$  (Fig. 2), we can calculate the total photon energy released from the Pop III stars. This can be done by supposing that each photon has an effective energy of  $E_\gamma = c_\gamma \int_{\nu_{\text{ion}}}^{\infty} d\nu h\nu B_\nu(T_*) / \int_{\nu_{\text{ion}}}^{\infty} d\nu B_\nu(T_*)$ , where  $h\nu_{\text{ion}} = 13.6 \text{ eV}$  and  $B_\nu(T_*)$  is the spectrum of a star with temperature  $T_*$ . The energy of the non-ionizing photons is included through  $c_\gamma = u_{\text{tot}}/u_{\nu > \nu_{\text{ion}}}$  ( $u$  is the energy from the star). A Pop III star has  $T_* \sim 80000 \text{ K}$  (Shioya et al. 2002, p. 9) which gives  $E_\gamma \approx 36 \text{ eV}$ . Note that for other reasonable star temperatures,  $E_\gamma$  does not vary significantly,  $E_{\gamma|60 \times 10^3 \text{ K}} \approx 36 \text{ eV}$  and  $E_{\gamma|100 \times 10^3 \text{ K}} \approx 40 \text{ eV}$ . Hence, the total Pop III photon energy production is  $E_\gamma \frac{dn_\gamma}{dz}/n_b$  per baryon per unit  $z$ . For each consumed nucleon, we assume that a nuclear energy of  $E_r = 7 \text{ MeV}$  is released as radiation, which means that the nucleon consumption rate is  $\frac{E_\gamma}{E_r} \frac{dn_\gamma}{dz}/n_b$  nucleons per baryon per unit  $z$ . If  $f_d$  is the fraction of the consumed baryon mass that becomes interstellar dust, (some of the metal atoms will remain with the core after the SN explosion, some will stay in the close vicinity of the SN and some will never clump together to form dust) the co-moving dust production rate will be

$$J_+ = f_d \frac{E_\gamma}{E_r} \Omega_b \frac{dn_\gamma}{dz} / n_b. \quad (4)$$

A dust grain will eventually be destroyed, e.g. by collision, by supernova shockwaves or by cosmic rays, see Draine & Salpeter (1979) for further discussion. If a dust grain has a lifetime of  $\Delta t$  we can write the dust destruction rate as

$$J_- = \frac{\Omega_{d,0}(z)}{\Delta t} \frac{dt}{dz} \approx - \frac{\Omega_{d,0}(z)}{\Delta t H_0 \Omega_m^{1/2} (1+z)^{5/2}}, \quad (5)$$

where  $\Omega_m$  is the relative matter content today, because the universe is matter dominated for  $5 < z < 15$ .

Solving Eq. (3) gives the dust density evolution

$$\Omega_{d,0}(z) = \int_z^{z_i} J_+(z') \frac{Y(z')}{Y(z)} dz', \quad (6)$$

where  $z_i = 20$  is the beginning of the dust formation (see Fig. 1) and

$$Y(z) = \exp\left(\frac{2}{3} \frac{(1+z)^{-3/2}}{\Omega_m^{1/2} \Delta t H_0}\right). \quad (7)$$

We note that the source term  $J_+$  is modulated by the destruction term  $\frac{Y(z')}{Y(z)}$ . The dust density is plotted in Fig. 3 where we note a strong dependency on the dust lifetime. In local dust  $\Delta t \sim 100 \text{ Myr}$ , Draine & Salpeter (1979). However, the uncertainty is rather large, according to Draine (1990),  $\Delta t = 30 \text{ Myr} - 10 \text{ Gyr}$ , depending on the environment. Note, however, that the density at the reionization red-shifts is much lower than in the interstellar medium in the Milky Way which implies a rather long dust life-time.



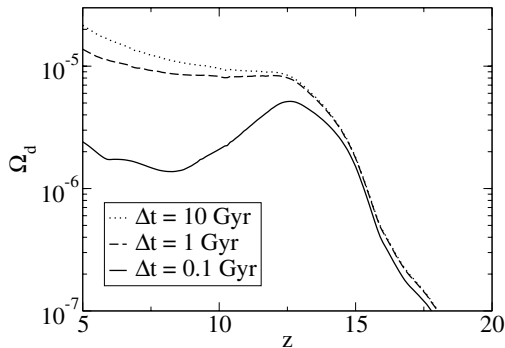


**Fig. 3.** The co-moving relative dust density evolution  $\Omega_{d,0} = \rho_{\text{dust}}/\rho_c$ , for  $f_d = 1$ . The minima at  $z = 6$  and  $9$  for  $\Delta t \leq 0.1$  Gyr is due to the fact that  $\Delta z = 1$  is not a constant time interval.

### 3. Results and discussion

#### 3.1. Metallicity

If we suppose that most of the metals were ejected as dust (not as gas) the metallicity comes from the dust grains. The metallicity is directly obtained through the produced dust. By letting  $\Delta t \rightarrow \infty$  ( $\Delta t = 10$  Gyr is good enough) we find the metallicity:

$$\frac{Z}{Z_\odot} = \frac{\Omega_{d,0}(\Delta t \rightarrow \infty)}{0.02 \cdot \Omega_b} \approx 1147 \cdot \Omega_{d,0}(\Delta t \rightarrow \infty) \quad (8)$$

or in absolute terms  $Z \approx 22.9\Omega_{d,0}$ . At  $z = 5$  we have  $\Omega_{d,0} = 2.3 \times 10^{-5} f_d$ , which gives  $Z \approx 5.2 \times 10^{-4} f_d = 0.026 f_d Z_\odot$ .

There are not much metallicity data available for  $z > 5$ . Metal poor stars in our galaxy are one point of reference, absorption lines in the Ly $\alpha$  spectrum from quasars are another one. The lowest metallicities found in stars in the Milky Way are  $Z/Z_\odot \sim 0.01$ , Depagne et al. (2002). The Ly $\alpha$  forest suggests (Songaila & Cowie 2002, Fig. 13) that  $Z/Z_\odot \sim 0.003$  for  $z \sim 4.5$  assuming that  $[\text{Fe}/\text{H}] \approx \log(Z/Z_\odot)$  as suggested by (VandenBerg et al. 2000, page 432). This indicates that  $f_d \sim 0.1$ . However, this might be lower than the actual value, cf. (Pettini et al. 1997, Fig. 4).

In heavy stars, virtually all the helium is consumed, producing metals. For simplicity (and lack of data), we assume that all the ejected metals clump to form dust,  $f_d \approx f_{\text{eject}}$ . This means that  $f_d$  will almost entirely depend on the dust ejection rate in the supernova explosion. In Iwamoto et al. (1998) a detected hypernova of mass  $M \sim 14 M_\odot$  seems to have  $f_{\text{eject}} \gtrsim 0.7$ . Furthermore, according to a dust production model by Nozawa et al. (2003),  $f_d \approx 0.2-0.3$ . At the same time, some of the stars will become black holes, not ejecting any metals, Heger & Woosley (2002), decreasing  $f_d$ . Currently this decrease is largely unknown.

In summary, the mass fraction of the produced metals in the Pop III stars, having become interstellar dust, should be around  $f_d \sim 0.1-0.3$ . In the following we use the more conservative  $f_d = 0.1$ , in agreement with the Ly $\alpha$  forest measurements, unless otherwise stated.

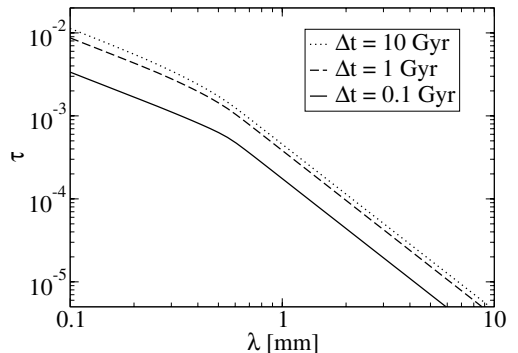


**Fig. 4.** Opacity  $\tau$  with dust evolution taken into account.

#### 3.2. Dust opacity

With our model for the dust density evolution, we want to calculate the opacity of the dust, as seen by the CMB. This will tell us how much the CMB spectrum is altered by the passage through the dust.

The dust opacity is given by

$$\begin{aligned} \tau_\nu &= c \int dz \frac{dt}{dz} \sigma_{\nu_e} n_d(z) \\ &= \frac{Q_0 c}{\sqrt{\Omega_m} a_r H_0} \frac{3 \rho_c}{4 \rho_g} \int dz \left( \frac{\nu}{\nu_r} \right)^{\beta_{\nu_e}} \Omega_{d,0}(z) (1+z)^{1/2+\beta_{\nu_e}}, \end{aligned} \quad (9)$$

where  $\nu$  ( $\nu_e$ ) is the observed (emitted) frequency and  $\nu = \nu_e/(1+z)$ . The dust number density is  $n_d(z) = (1+z)^3 \times \rho_c \Omega_{d,0}(z)/m_g$  where  $m_g = \frac{4\pi a^3}{3} \rho_g$  is the grain mass. We see (from  $\tau \propto \Omega_{d,0}$ ) that  $\tau$  is proportional to the parameter  $f_d$ .

The resulting opacity can be seen in Fig. 4. We note that the opacity is small,  $\tau \ll 1$ . The smooth knee is due to the change of  $\beta$  at the redshifted  $\nu_r$ , see Sect. 2, but this is not in the spectral range of the CMB. The differential opacity  $d\tau/dz$  is plotted in Fig. 5 for  $\lambda = 1$  mm. We see that with a short dust lifetime, the dust differential opacity falls off almost immediately (in terms of  $z$ ). However, for longer lifetimes, the early dust could still play a certain role for  $z < 3$ . This could eventually contribute to dimming of distant objects. We also note the impact of the expansion of the universe in decreasing the dust density and thus the opacity. This is why the increase in Fig. 1, at  $z \sim 5$ , is not apparent in the opacity, Fig. 4. Furthermore, the submillimetre effective dust opacity follows a  $\nu^2$  emissivity law.

#### 3.3. Dust temperature

In order to deduce the equilibrium temperature of the dust, we write the balance between the absorbed CMB, the absorbed starlight and the emitted IR light from the dust:

$$P_d = P_* + P_{\text{CMB}}. \quad (11)$$

The powers  $P_d$  and  $P_{\text{CMB}}$  can be written as

$$P_X = 4\pi \int_0^\infty d\nu_e \sigma_{\nu_e} B_{\nu_e}(T_X), \quad (12)$$

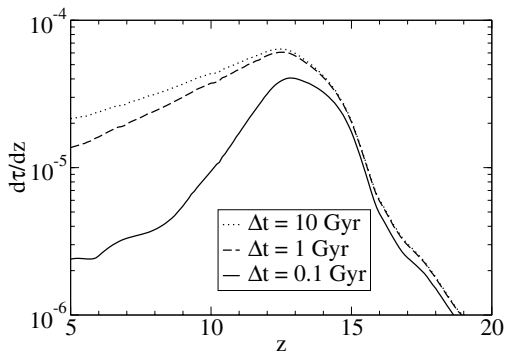


**Fig. 5.** The differential opacity  $d\tau/dz$  at  $\lambda = 1$  mm for different dust lifetimes.

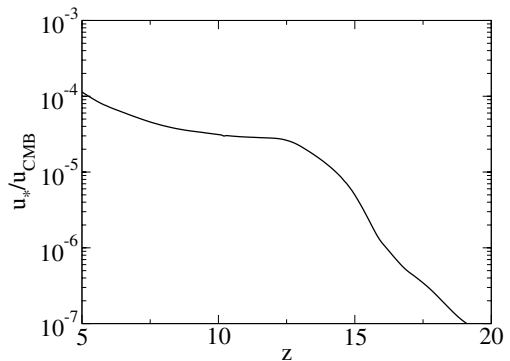


**Fig. 6.** Energy density of ionizing photons compared to  $u_{\text{CMB}} = 4\sigma_{\text{S}}T_{\text{CMB}}^4/c$ , where  $\sigma_{\text{S}}$  is Stefan-Boltzmann's constant.

where  $B_\nu$  is a Planck blackbody spectrum and  $X = \{\text{CMB}, \text{d}\}$ . In the wave-length range considered, the spectral index  $\beta = 2$ . Supposing that  $\beta$  is constant, Eq. (11) can be solved for the dust temperature analytically in the submm range:

$$T_{\text{d}}^{4+\beta} = T_{\text{eff}}^{4+\beta} + T_{\text{CMB}}^{4+\beta}, \quad (13)$$

where the effective temperature is defined by

$$T_{\text{eff}}^{4+\beta} = \frac{P_*}{8\pi^2 hc^{-2} (Q_0 \cdot (a^3/a_r) \nu_r^{-\beta}) (k_{\text{B}}/h)^{4+\beta} C_\beta} \quad (14)$$

and  $C_\beta = \int_0^\infty dx x^{3+\beta} / (e^x - 1) = (\beta + 3)! \sum_{k=1}^\infty k^{-(4+\beta)}$ , such that  $C_0 \approx 6.494$ ,  $C_1 \approx 24.89$  and  $C_2 \approx 122.1$ .

However, in our calculations we use the exact Eqs. (11) and (12), while Eq. (14) can be used as a cross-check.

The absorbed power density,  $P_*$  from the radiation of Pop III stars peaks in the UV-region and can be approximated by

$$P_* = \sigma_{\text{UV}} u_*(z), \quad (15)$$

where  $\sigma_{\text{UV}}$  is the dust-photon cross section in the UV region and the energy density is

$$u_*(z) = f_{\text{esc}} \int_{z_i}^z dz' \frac{dn_\gamma}{dz'} E_\gamma \left( \frac{1+z}{1+z'} \right)^4, \quad (16)$$

where  $f_{\text{esc}}$  is the escape fraction of photons from the star halos. We neglect the loss of photons due to the reionization itself.  $E_\gamma \frac{1+z}{1+z'}$  is the effective energy of the photon emitted at  $z'$  and then redshifted to  $z$ . According to Cen (2003),  $f_{\text{esc}} = 0.3$  gives an electron opacity  $\tau_e \approx 0.13$  which is within one standard deviation of the results by WMAP. Hereafter, we adopt this value of  $f_{\text{esc}}$ .

The energy density of the ionizing photons are compared to the CMB in Fig. 6. The star energy density is much less than the CMB energy density at this epoch, and the curve resembles the accumulated photons in Fig. 1. Hence, the dust temperature closely follows the CMB temperature, see Fig. 7 and Eq. (12).

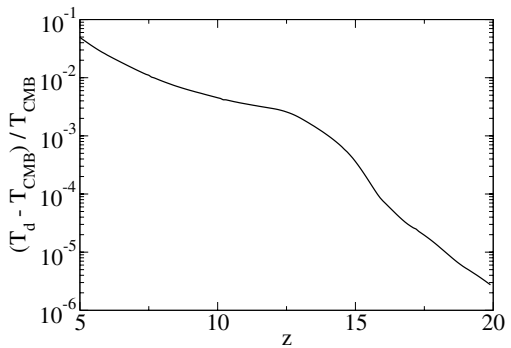


**Fig. 7.** The dust temperature is plotted against the CMB temperature with the relative quantity  $(T_{\text{d}} - T_{\text{CMB}})/T_{\text{CMB}}$ .

### 3.4. Observed intensity

Now we proceed to compute the average intensity (monopole term) of the submm and microwave background which is made of the CMB and early dust emission. The simple radiative transfer of the CMB through the uniform dust screen yields the following observed intensity:

$$i_\nu = e^{-\tau_\nu} \left[ B_\nu(T_{\text{CMB}}) + \int_0^{\tau_\nu} e^{\tau_e} \frac{B_\nu(T_{\text{d}}(z))}{(1+z)^3} d\tau_e \right]. \quad (17)$$

From Figs. 4 and 7, we see that the opacity is small, ( $\tau \ll 1$ ) and the dust temperature is only slightly higher than the CMB temperature ( $T_{\text{d}} \gtrsim T_{\text{CMB}}$ ). This gives the following formula for the excess intensity relative to the unperturbed CMB:

$$\begin{aligned} \Delta i_\nu &\equiv i_\nu - B_\nu(T_{\text{CMB}}) \\ &\approx T_{\text{CMB}} \frac{dB_\nu}{dT} \Big|_{T=T_{\text{CMB}}} \int_0^{\tau_\nu} \frac{T_{\text{d}}(z) - T_{\text{CMB}}(z)}{T_{\text{CMB}}(z)} d\tau_e, \end{aligned} \quad (18)$$

where  $T_{\text{CMB}}$  is the CMB temperature today. The integrand is plotted in Fig. 7. We note that a new component is added to the primary CMB spectrum. Equation (18) tells us that it has a

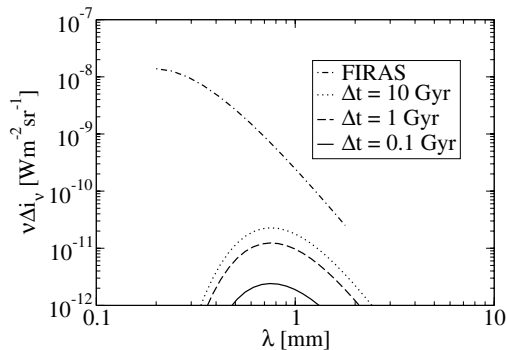


**Fig. 8.** Comparison of the modeled intensity for the early dust emission in excess of the CMB with the observed FIRAS spectrum (dashed red curve) of the cosmic far IR background as detailed by Lagache et al. (1999).

specific spectrum which is the product of a 2.725 K blackbody temperature fluctuation spectrum (like primary anisotropies) and a  $\nu^2$  power law (from  $d\tau_e$ ). This effect is mostly visible in the submm range and has a minor contribution in the radio domain.

In Fig. 8, the excess intensity is plotted along with the extragalactic background measured by FIRAS, Puget et al. (1996); Fixsen et al. (1998); Lagache et al. (1999). Depending on the dust destruction rate (parametrized by the dust lifetime  $\Delta t$ ), the computed early dust background can be an important part of the observed background from 400  $\mu\text{m}$  up to the mm wave-length. The exact position of  $\lambda_r$  will only slightly displace the spectrum, leaving the magnitude unchanged. Most of the far IR background can now be explained by a population of  $z = 0$  to  $z = 3$  luminous IR galaxies, Gispert et al. (2000). A fraction of the submillimetre part of this background could arise from larger redshift dust emission as suggested by Fig. 8.

In order to check our results, we calculate the co-moving luminosity density of the dust in the submm region and compare it with (Gispert et al. 2000, Fig. 4). We find them compatible.

### 3.5. Discussion

Just like the Thomson scattering during reionization, early dust will also tend to erase the primordial anisotropies in the CMB. However, due to the much smaller dust opacity (compare  $\tau_d(1 \text{ mm}) \lesssim 10^{-3}$  and  $\tau_e = 0.17$ ), this effect will be negligible.

The early dust will also introduce a new type of secondary anisotropies with a typical size of a dark matter filament. Here, we only estimate the order of magnitude of this effect. If the co-moving size of the dark matter filament is  $L$ , the angular size is  $3 \cdot (L/5 \text{ Mpc})$  arcminutes at  $z = 10$  which corresponds to multipole number  $\ell \sim 4000 \cdot (L/5 \text{ Mpc})$ . Fortunately, this region in  $\ell$ -space does not contain any primordial fluctuations because of the Silk damping. However, there are other foregrounds in the same region, see Aghanim et al. (2000).

If we suppose a contrast of 10% in the dust intensity between dark matter filaments and the void, we obtain values of  $\Delta T/T \approx 3 \times 10^{-7}$  (for  $\lambda = 1 \text{ mm}$ ,  $f_d = 0.1$  and  $\Delta t = 1 \text{ Gyr}$ ). These anisotropies, pending more accurate calculations, clearly are in the range of expected arcminute secondary anisotropies from other effects. They could be detected by Planck HFI (High Frequency Instrument), Lamarre et al. (2003) and FIRAS-II type of instrument, Fixsen & Mather (2002).

The results of these calculations depend only very weakly on the precise dust model assumptions. We have also tried a different (but similar) shape of the ionizing photon production, Fig. 1, and found that the results do not vary significantly.

Very little is known about the universe during the reionization epoch. Nevertheless, there are several parameters that could be calculated more accurately.

The two most important parameters in the present model are the dust lifetime,  $\Delta t$  and the mass fraction of the produced metals that are ejected as interstellar dust,  $f_d$ . The dust lifetime could be determined more precisely by making 3D simulations of the dust production in combination with structure formation. The simulations would also give the inhomogeneous dust density evolution. The result would be a better estimate of the aforementioned secondary anisotropies caused by the variations in the dust opacity. A more refined dust grain model, using e.g. a distribution of grain sizes would also be more realistic. If the dust is long-lived, it could also have a certain impact on measurements in the optical and UV region. Finally, we note that most of the results are proportional to the dust density and thus to  $f_d$ . To evaluate  $f_d$  more precisely, we need a better understanding of the typical properties of the first generation of stars, see Sect. 3.1, which is currently much debated.

## 4. Conclusions

We have shown that the radiation from early dust, produced and heated by Pop III stars, contributes to the extragalactic submillimetre background within the limits set by FIRAS. It may not be detected by the present generation of instruments but future experiments such as Planck HFI and FIRAS-II should be able to measure it, by using its specific predicted spectral signature. This high-redshift dust, contemporary to the reionization, should show up as small-scale anisotropies when observed by sensitive submillimetre instruments. These anisotropies are in the same range as other small-scale anisotropy effects.

## References

- Aghanim, N., Balland, C., & Silk, J. 2000, *A&A*, 357, 1
- Boulanger, F., Abergel, A., Bernard, J.-P., et al. 1996, *A&A*, 312, 256
- Cen, R. 2002, *ApJ*, 591, 12
- Cen, R. 2003, *ApJ*, 591, L5
- Depagne, E., Hill, V., Spite, M., et al. 2002, *A&A*, 390, 187
- Désert, F.-X., Boulanger, F., & Puget, J. L. 1990, *A&A*, 237, 215
- Draine, B. T. 1990, in *The Evolution of the Interstellar Medium*, ASP Conf. Ser., 12, 193
- Draine, B. T., & Salpeter, E. E. 1979, *ApJ*, 231, 438

- Fixsen, D. J., Dwek, E., Mather, J. C., Bennett, C. L., & Shafer, R. A. 1998, *ApJ*, 508, 123
- Fixsen, D. J., & Mather, J. C. 2002, *ApJ*, 581, 817
- Gispert, R., Lagache, G., & Puget, J. L. 2000, *A&A*, 360, 1
- Heger, A., & Woosley, S. E. 2002, *ApJ*, 567, 532
- Iwamoto, K., Mazzali, P. A., Nomoto, K., et al. 1998, *Nature*, 395, 672
- Kogut, A., Spergel, D. N., Barnes, C., et al. 2003, *ApJS*, 148, 161
- Lagache, G., Abergel, A., Boulanger, F., Désert, F. X., & Puget, J.-L. 1999, *A&A*, 344, 322
- Lamarre, J. M., Puget, J. L., Bouchet, F., et al. 2003, [[arXiv:astro-ph/0308075](#)]
- Nozawa, T., Kozasa, T., Umeda, H., Maeda, K., & Nomoto, K. 2003, [[arXiv:astro-ph/0307108](#)]
- Pei, Y. C., Fall, S. M., & Hauser, M. G. 1999, *ApJ*, 522, 604
- Pettini, M., Smith, L. J., King, D. L., & Hunstead, R. W. 1997, *ApJ*, 486, 665
- Puget, J.-L., Abergel, A., Bernard, J.-P., et al. 1996, *A&A*, 308, L5
- Shioya, Y., Taniguchi, Y., Murayama, T., et al. 2002, *ApJ*, 576, 36
- Songaila, A., & Cowie, L. L. 2002, *AJ*, 123, 2183
- Spergel, D. N., Verde, L., Peiris, H. V., et al. 2003, *ApJS*, 148, 175
- VandenBerg, D. A., Swenson, F. J., Rogers, F. J., Iglesias, C. A., & Alexander, D. R. 2000, *ApJ*, 532, 430

---

# Paper II

---

## **Dust Distribution during Reionization**

The spatial distribution of the dust is estimated using simulations of dark matter density evolution. Combining the calculated intensity from Paper I with this density and integrating along the line of sight, the spatial signature of the dust is obtained.

Elfgren, Erik, Désert, François-Xavier, Guiderdoni, Bruno, Submitted to Astronomy and Astrophysics.



# Dust Distribution during Reionization

Erik Elfgrén<sup>1</sup>, François-Xavier Désert<sup>2</sup>, and Bruno Guiderdoni<sup>3</sup>

<sup>1</sup> Department of Physics, Luleå University of Technology, SE-971 87 Luleå, Sweden

<sup>2</sup> Laboratoire d'Astrophysique, Observatoire de Grenoble, BP 53, 414 rue de la piscine, 38041 Grenoble Cedex 9, France

<sup>3</sup> Observatoire de Lyon, 9, avenue Charles Andr, 69561 St-Genis Laval Cedex, France

Received  $\ddot{date}_r$  / Accepted  $\ddot{date}_c$

**Abstract.** The dust produced by the first generation of stars will block the Cosmic Microwave Background to some extent. In order to evaluate this, we calculate the power spectrum of the dust and show that this dust might be detectable with the Planck satellite at small angular scales ( $\ell \gtrsim 1000$ ). The power spectrum of the dust is compared with errors of Planck and is found to be noticeable for certain values of dust lifetime and dust production rates.

**Key words.** Dust – CMB – Reionization - Power spectrum

## 1. Introduction

The importance of the Cosmic Microwave Background (CMB) as a cosmological tool has been demonstrated thoroughly during the last few years. It has been used to evaluate the age of the universe, the Hubble parameter, the baryon content, the flatness and the optical depth of the reionization, Bennett et al. (2003); the non-Gaussianity of the primary fluctuations, Komatsu et al. (2003); the Sunyaev-Zeldovich fluctuations from the first stars, Oh et al. (2003); the primordial magnetic fields, Subramanian et al. (2003); the spatial curvature of the universe, Efstathiou (2003); the formation of population III stars, Cen (2003); and the neutrino masses, Hannestad (2003).

However, in order to interpret the CMB signal correctly, its foreground must also be well known.

In this paper we focus on one particular aspect of the foreground of the CMB: the primordial dust. This dust was created during the reionization period in the first generation of stars and was then ejected into the interstellar medium (ISM). The dust will therefore partly block the path of the CMB photons and slightly deform the spectrum. As we have shown in an earlier paper Elfgrén & Désert (2004), this dust has a characteristic spectrum proportional to a primary anisotropy ( $\Delta T$ ) spectrum times the frequency squared. The dust spectrum was shown to be lower than the CMB by roughly two orders of magnitude because the heating from the stars is significantly less than that of the CMB at the time.

Nevertheless, the dust will also have a characteristic spatial distribution which could be used to identify its signal. The objective of this paper is to determine this distribution and its impact on different measurements of the CMB. Of particular interest is the Planck satellite mission, but also other instru-

ments, like MAMBO and BLAST could be interesting. The spatial distribution is estimated from the GalICS (Galaxies In Cosmological Simulations)  $N$ -body simulations of dark matter, which are described in more detail in section 2. The dust distribution is then combined with the intensity of the dust emission as calculated in Elfgrén & Désert (2004), and this is integrated along the line of sight. The resulting power spectrum is then plotted in terms of the spherical harmonics  $C_\ell$  and compared with detection limits of Planck.

In our model, we assume a  $\Lambda$ CDM universe with  $\Omega_{tot} = \Omega_m + \Omega_\Lambda = 1$ , where  $\Omega_m = \Omega_b + \Omega_{DM} = 0.133/h^2$ ,  $\Omega_b = 0.0226/h^2$  and  $h = 0.72$  as advocated by WMAP, Spergel et al. (2003), using WMAP data in combination with large scale structure observations (2dFGRS + Lyman  $\alpha$ ).

## 2. Dark Matter Simulations

The distribution of dark matter in the universe was calculated using the GalICS program. The cosmological  $N$ -body simulation we refer to throughout this paper was done using the parallel tree-code developed by Ninin (1999). The power spectrum was set in agreement with Eke et al. (1996):  $\sigma_8 = 0.88$ , and the Dark Matter (DM) density field was calculated from  $z=35.59$  to  $z=0$ , outputting 100 snapshots spaced logarithmically in the expansion factor.

GalICS is a hybrid model for hierarchical galaxy formation studies, combining the outputs of large cosmological  $N$ -body simulations with simple, semi-analytic recipes to describe the fate of the baryons within dark matter halos. The simulations produce a detailed merging tree for the dark matter haloes, including complete knowledge of the statistical properties arising from the gravitational forces.

The basic principle of the simulations is to randomly distribute a number of dark matter particles  $N^3$  with mass  $M_{DM}$

in a box of size  $L^3$ . Then, as time passes, the particles interact gravitationally, clumping together and forming structures. The clumps of Dark Matter are called halos and in our simulation we require at least 5 particles to clump together before we call it a halo. There are supposed to be no other forces present than the gravitation and the boundary conditions are assumed to be periodic.

In the simulations we used, the side of the box of the simulation is  $L = 100h^{-1}$  Mpc and the number of particles are  $256^3$  which implies a particle mass of  $\sim 5.51 \times 10^9 h^{-1} M_\odot$ . Furthermore, the cosmological parameters were  $\Omega_\Lambda = 2/3$ ,  $\Omega_m = 1/3$  and  $h = 2/3$ . Between the assumed initial dust formation at  $z \sim 15$  and the end of this epoch in the universe at  $z \sim 5$ , there are 51 snapshots. In each snapshot a friend-of-friend algorithm was used to identify virialized groups of at least five DM particles. The number of particles have been set low in order to produce halos already at  $z = 14.7$ .

In order to make a correct large-scale prediction of the distribution of the Dark Matter and therefore the dust, the size of the box would have to be of Hubble size, i.e. 3000 Mpc. However, increasing the size of the box and maintaining the same number of particles would mean that we loose in mass resolution, which is not acceptable if we want to reproduce a fairly realistic scenario of the evolution of the universe.

There is another way to achieve the desired size of the simulation without loosing in detail or making huge simulations. This method is called MoMaF (Mock Map Facility) and is described in detail in Elfgren (2002). The basic principle is to use the same box, but at different stages in time and thus a cone of the line of sight can be established. In order to avoid replication effects, the periodic box is randomly rotated for each time-step. This means that there will be loss of correlation information on the edges of the box, since those parts will be gravitationally disconnected from the adjacent box. Fortunately, this loss will only be of the order of 10% as shown in Elfgren (2002).

### 2.1. Validity of Simulation

The distribution of galaxies resulting from this GALICS simulation has been compared with the 2dS Colless et al. (2001) and the Sloan Digital Sky Survey Szapudi et al. (2001) and found to be realistic on the angular scales of  $3' \lesssim \theta \lesssim 30'$ , see Elfgren (2002). The discrepancy in the spatial correlation function for other values of  $\theta$  can be explained by the limits of the numerical simulation. Obviously, any information on scales larger than the size of the box is not reliable. Since the simulation gives reasonable predictions of the matter distributions today, it seems likely that it is also valid at higher  $z$  when the early dust is produced.

## 3. Model

Since very little is known about the actual distribution of the dust throughout the universe at this time, we simply assume that the dust distribution follows the dark matter distribution. We propose two different ways for this to happen and explore these. The first is to let the dust be proportional to the dark matter halos, the second is to make a hydrodynamical smoothing

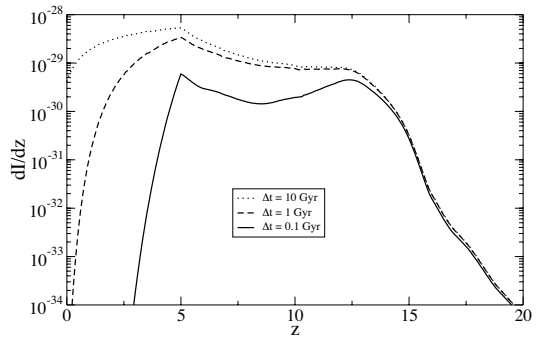


Fig. 1. Intensity contribution from the dust per time-step  $z$ .

of the dark matter density field and set the dust density proportional to this density:

$$\rho_{dust}(\mathbf{r}, z) \propto \rho_{DM}(\mathbf{r}, z), \quad (1)$$

where  $\rho_{DM}$  represents either the Halo method or the Smoothing method. We will focus on the Halo method since it is more likely that the dust will have formed in galaxies and halos than that it will have formed anywhere that there is dark matter.

In order to estimate the measured intensity, we need to do this distribution in terms of this intensity instead. In our previous paper, Elfgren & Désert (2004), we calculated the intensity as a function of redshift, supposing that none of the light emitted from the stars is absorbed. This is close enough to the truth since there are more than 100 ionizing photons produced per baryon. The result is plotted in Fig. 1.

In our present model, the dust intensity is spatially distributed such that

$$\frac{dl}{dz}(\mathbf{r}, z) \propto \rho_{DM}(\mathbf{r}, z). \quad (2)$$

The MoMaF method (section 2) is then used to project the emitted intensity from the dust on a  $45^\circ \times 45^\circ$  patch along the line of sight. Within each box equation 2 is normalized to produce  $\int_{\text{box depth}} dl/dz(z)$  when averaged over the projected box. If a box is deeper than the time-step is long, the box is simply chopped there. For  $z < 2.3$ , the time-step is too short but this is of little consequence since the dust density is so low at this time. The box is divided into a grid according to the resolution that we wish to test. For Planck this means a grid that is  $9 \times 9$  pixels, for SCUBA  $45 \times 45$ .

To check the resulting intensity image, we have calculated its  $\sum dl_{x,y}/N_{pix}^2$  and found it to be equal to  $\int dl(z)dz$  to within a few per cent.

## 4. Results and Discussion

As described above, the MoMaF technique produces an image of the line of sight. This image represents the patch of the sky covered by the box, 150 co-moving  $\text{Mpc}^2$  which translates to  $\sim 45^\circ$  and is apodized (smoothed on the edges), so as to avoid



artifacts on the edges. Thereafter the image is Fourier transformed into frequency space  $P_k$ . In order to convert this spectrum into spherical harmonics correlation function we apply the following transformation:

$$\ell = k \cdot (2\pi) / (4 \cdot \sin(\theta/4)) \cdot N_{map} / N_{fft} \quad (3)$$

$$C_\ell = \theta^2 C_k. \quad (4)$$

These  $C_\ell$  is then calculated in units of  $[\mu\text{K}^2/B_\nu(T_{CMB})]$  at a frequency  $\nu = 353$  GHz (one of the Planck detectors work at this frequency). As discovered in Elfgren & Désert (2004), the intensity is proportional to the frequency squared which means that the power spectrum at a frequency  $\nu$  will be

$$C_\ell(\nu) = C_\ell(353 \text{ GHz}) \cdot \left(\frac{\nu}{353 \text{ GHz}}\right)^4. \quad (5)$$

In order to estimate an average power spectrum, 400 such images were generated and the  $C_\ell$  were averaged of these. For comparison, we also tried to paste all these images together and calculate the  $C_\ell$  for this (180×180 pixels) image. The result was very similar to the average  $C_\ell$ . To validate our results, we have also calculated the r.m.s. of the images and compared with  $\sum_\ell \frac{2\ell+1}{4\pi} C_\ell$  and found them to be compatible. The resulting power spectra can be seen in Fig. 2. As described in Elfgren & Désert (2004), the lifetime of these dust particles is a largely unknown factor and we plot three different lifetimes, 0.1, 1, 10 Gyrs. Furthermore, the intensity is proportional to the fraction of the formed metals that actually end up as dust, which we assumed to be  $f_d = 0.3$ . This means that the intensity  $C_\ell(f_d) = C_\ell(f_d = 0.3) \cdot f_d^2$ . We note that there is only a small difference between dust lifetimes of 10 Gyrs and 1 Gyr, while the 0.1 Gyr is lower by a factor four. The lowest curve in the figure represents the hydrodynamical smoothing method of distributing the dust for a dust lifetime of 1 Gyr. Naturally, it is significantly lower than the corresponding Halo method  $C_\ell$ :s because the DM halos will be much more grainy (especially early in the history) than the smoothed DM field. The difference between the two methods is a factor of  $\sim 10$  but they do not have exactly the same form.

The dust frequency spectrum will be distinctly different from that of other sources in the same frequency range. As shown in Elfgren & Désert (2004), it will be  $\propto \nu^2$ . We compare this spectrum with that of the CMB  $\Delta T/T$  and that of galactic dust,  $T=17$  K, Boulanger et al. (1996). In order to focus on the forms of the spectra, we normalize the three curves to one at  $\nu = 353$  GHz. The result is presented in Fig. 3. In case of a weak dust signal, this frequency signature could allow us to distinguish the dust signal from the CMB and other foregrounds.

#### 4.1. Detection with Planck?

The Planck satellite, due for launch in 2007, will have an angular resolution of  $\sim 5'$  and will cover the whole sky. Our simulated box of  $45'^2$  will thus correspond to  $9 \times 9$  pixels in Planck. Correlations on larger angular scales than  $45'$  will not be available from our simulations. However, the dust correlations will

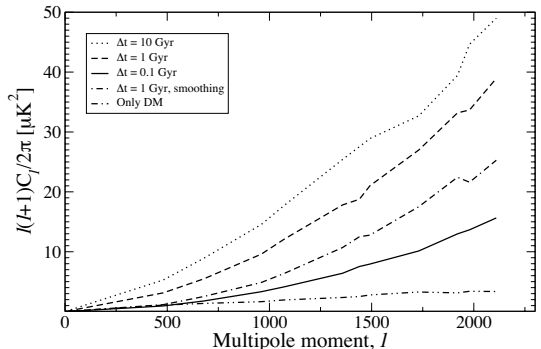


**Fig. 2.** Dust power spectrum at 353 GHz for a map  $45' \times 45'$  and Planck resolution  $5'$  for three different lifetimes for the dust particles, 0.1, 1, 10 Gyrs, with a solid, dashed and dotted line respectively. The dash-dash-dot line represents the normalized correlation for the DM halos only without dust. The DM smoothing method for a dust lifetime of 1 Gyr is the dot-dot-dot line. We note that the DM smoothing method gives correlations that are approximately a factor ten lower than the DM halo method. Also, the form is not quite the same.

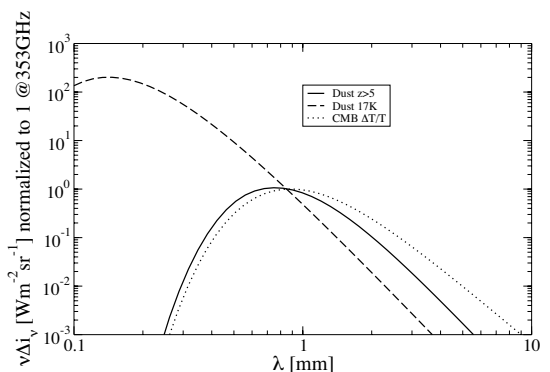


**Fig. 3.** The form of the early dust spectrum compared to the form of galactic dust (with a temperature of 17K) and the CMB. The curves have been normalized to 1 at 353 GHz. We see that the early dust has a special spectral signature.

increase at smaller angles while the CMB and many other signals will decrease. This means that our lack of information on angular scales  $\ell \lesssim 250$  will not be of any consequence, as can be seen in Fig. 4. Planck will measure the CMB at  $\nu = 100, 143, 217, 353, 545, \text{ and } 857$  GHz. We have chosen  $\nu = 353$  as our reference frequency. At higher frequencies, the galactic dust will become more of a nuisance and at lower frequencies the CMB primary anisotropies will tend to dominate. To transpose to other frequencies, recall from Eq. 5, that  $C_\ell \propto \nu^4$ .

In order to test to detectability of the dust with Planck, we evaluate the total error

$$E = \sqrt{\frac{2}{(2\ell + 1)f_{cut}L}} \times (E_{CMB} + E_{instrument}), \quad (6)$$

Frequency [GHz]	100	143	217	353	545	857
$FWHM [']$	9.5	7.1	5.0	5.0	5.0	5.0
$s_X [\mu\text{Ks}^{1/2}]$	32.0	21.0	32.3	99.0	990	45125

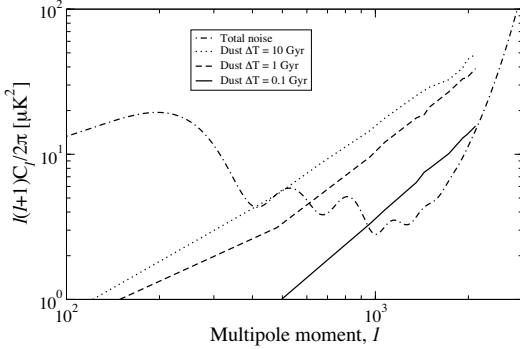


**Fig. 4.** Comparison between dust power spectrum and Planck error limits at 353 GHz with binning 500. The error limits (total noise) consist of two parts; the CMB cosmic variance, which dominates for small  $\ell$  and the instrument noise, which dominates for high  $\ell$ .

where  $f_{cut} = 0.8$  is the percentage of the sky used,  $L$  is the bin-size,  $E_{CMB}$  is the cosmic variance and the instrument error is

$$E_{instrument} = f_{sky} \frac{4\pi s_X^2}{t_{obs}} \cdot e^{\ell^2 - \sigma_b^2} \cdot \frac{\ell(\ell+1)}{2\pi}, \quad (7)$$

where  $f_{sky} = 1$  is the percentage of the sky covered,  $s_X$  is the noise per second  $[\mu\text{Ks}^{1/2}]$ ,  $t_{obs} = 14 \cdot 30 \cdot 24 \cdot 3600$  s is the observation time (14 months), and  $\sigma_b = FWHM/2.35$  is the lobe sensitivity in radians ( $FWHM = \text{Full Width Height Median}$ ).

For Planck, the values of these parameters are given in table 4.1. The values of the cosmic variance  $E_{CMB}$  has been taken from the Lambda web-site (1 Mars 2005).

The resulting error for a binning of  $L = 500$  along with the dust power spectrum is plotted in figures 4-8. In figure 4, the frequency  $\nu = 353$  GHz is fixed while  $\ell$  is varied. We note that  $\ell \sim 1000$  seems to be a good place to search for dust. At low  $\ell$ , the error due to the cosmic variance dominates, at high  $\ell$  the instrument noise.

In figures 5 – 8, the binning center is fixed for each figure while the Planck frequencies constitutes the variable. The fourth point in the figures correspond to  $\nu = 353$  GHz and apparently gives the best signal over error ratio. At low frequencies the cosmic variance is important, at high frequencies, the instrument error.

## 4.2. Discussion

The First we compare with SCUBA measurements, see Borys et al. (1999), and find that  $\ell(\ell+1)C_\ell^{Dust}/2\pi$  at the mean  $\ell = 13081$  of SCUBA is  $\sim 1000 \mu\text{K}^2$ , see 9, which is much less than  $\ell(\ell+1)C_\ell^{SCUBA}/2\pi|_{\ell=13081} \approx 55450 \mu\text{K}^2$ . This means that the dust signal is too weak to have been detected by SCUBA.

Other detectors that might be of interest are FIRAS II, Fixsen & Mather (2002) BLAST, Devlin (2001) and MAMBO,

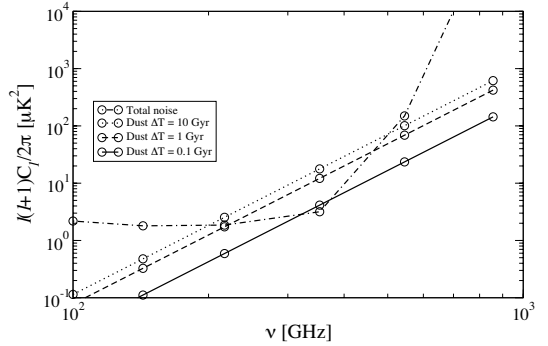


**Fig. 5.** Comparison between dust power spectrum and Planck error limits at  $\ell=1073$  with binning 500. The error limits (total noise) consist of two parts; the CMB cosmic variance, which is constant ( $\approx 1.7$ ) and the instrument noise that has a “U-shape”.

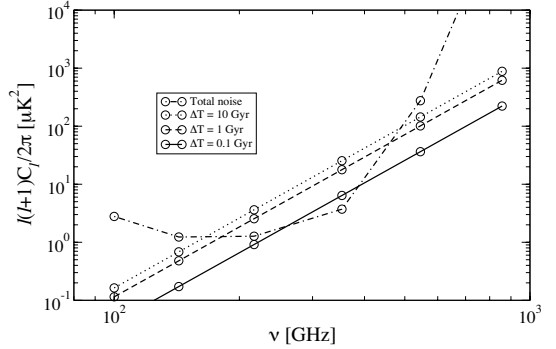


**Fig. 6.** Comparison between dust power spectrum and Planck error limits at  $\ell=1358$  with binning 500. The error limits (total noise) consist of two parts; the CMB cosmic variance, which is constant ( $\approx 1.0$ ) and the instrument noise that has a “U-shape”.

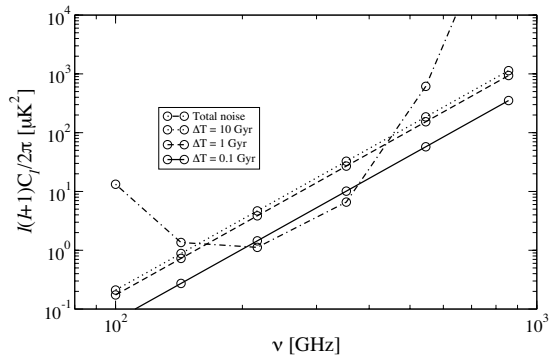


**Fig. 7.** Comparison between dust power spectrum and Planck error limits at  $\ell=1731$  with binning 500. The error limits (total noise) consist of two parts; the CMB cosmic variance, which is constant ( $\approx 0.47$ ) and the instrument noise that has a “U-shape”.

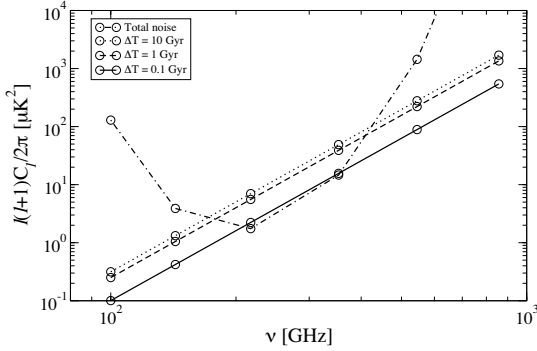


**Fig. 8.** Comparison between dust power spectrum and Planck error limits at  $\ell=2110$  with binning 500. The error limits (total noise) consist of two parts; the CMB cosmic variance, which is constant ( $\approx 0.21$ ) and the instrument noise that has a “U-shape”.

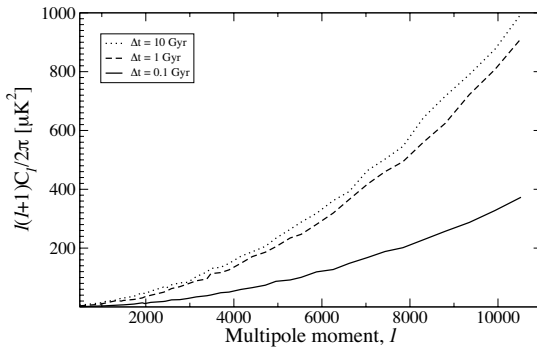


**Fig. 9.** Dust power spectrum as a function of multipole moment,  $\ell$ , for a map  $45' \times 45'$  and SCUBA resolution,  $1'$

Greve et al. (2004). BLAST will have a resolution of  $\sim 0.5'$  and a sensitivity which is a factor two lower than SCUBA's.

As a final remark, we note that other signals that are correlated with structures will also show a similar behavior in the power spectrum.

## 5. Conclusions

There seems to be a possibility to detect the dust from the first generation of stars with the Planck satellite on small angular scales ( $\ell \gtrsim 1000$ ). However, the detectability depends on the actual distribution of dust in the early universe, but also to a large extent on the dust lifetime. The results are parametrized so that changing the frequency and the fraction of produced metals that become dust is only a matter of scaling the figures. The spectral shape of the early dust is compared to that of the primary CMB anisotropies as well as local dust and found to have a unique signature.

## References

Bennett, C. L., Halpern, M., Hinshaw, G., et al. 2003, ApJS,

- 148, 1  
 Borys, C., Chapman, S. C., & Scott, D. 1999, MNRAS, 308, 527  
 Boulanger, F., Abergel, A., Bernard, J.-P., et al. 1996, A&A, 312, 256  
 Cen, R. 2003, ApJL, 591, L5  
 Colless, M., Dalton, G., Maddox, S., et al. 2001, MNRAS, 328, 1039  
 Devlin, M. 2001, in Deep Millimeter Surveys: Implications for Galaxy Formation and Evolution, 59–66  
 Efstathiou, G. 2003, MNRAS, 343, L95  
 Eke, V. R., Cole, S., & Frenk, C. S. 1996, MNRAS, 282, 263  
 Elfgren, E. 2002, ArXiv Astrophysics e-prints, hep-ph/0209238,, 1  
 Elfgren, E. & Désert, F.-X. 2004, A&A, 425, 9  
 Fixsen, D. J. & Mather, J. C. 2002, ApJ, 581, 817  
 Greve, T. R., Ivison, R. J., Bertoldi, F., et al. 2004, MNRAS, 354, 779  
 Hannestad, S. 2003, Journal of Cosmology and Astro-Particle Physics, 5, 4  
 Komatsu, E., Kogut, A., Nolta, M. R., et al. 2003, ApJS, 148, 119  
 Lambda web-site. 1 Mars 2005, <http://lambda.gsfc.nasa.gov>  
 Ninin, S. 1999, PhD thesis: Université Paris 11  
 Oh, S. P., Cooray, A., & Kamionkowski, M. 2003, MNRAS, 342, L20  
 Spergel, D. N., Verde, L., Peiris, H. V., et al. 2003, ApJS, 148, 175  
 Subramanian, K., Seshadri, T. R., & Barrow, J. D. 2003, MNRAS, 344, L31  
 Szapudi, I., Bond, J. R., Colombi, S., et al. 2001, in Mining the Sky, 249